Design and Analysis of Superlattices with Tailored Thermal Transport Properties

A thesis proposal by

Eric S. Landry

April 25, 2008

224 Scaife Hall

Department of Mechanical Engineering

Carnegie Mellon University

Thesis Committee

Assistant Professor Alan McGaughey (Committee Chair), Mechanical Engineering

Professor Shi-Chune Yao, Mechanical Engineering

Professor Sara Majetich, Physics

Dr. Marcela Madrid, Pittsburgh Supercomputing Center

Contents

1 Introduction

1.1 Motivation

Superlattices are periodic nanostructures containing alternating material layers with thicknesses as small as a few nanometers (see Fig. 1).[1–8] Traditionally, these structures have been designed for control of electron and photon transport.[9–11] The thermal transport by phonons, however, can also be controlled through the proper design of the superlattice unit cell. In the past decade, semiconductor superlattices (e.g., $Si/Si_{1-x}Ge_x$, GaAs/AlAs, and Bi_2Te_3/Sb_2Te_3) have been examined as candidates for improving the efficiency of thermoelectric energy conversion. This is because the superlattice cross-plane thermal conductivity can be reduced while maintaining good electron transport properties, resulting in high values of the thermoelectric figure-of-merit, ZT.[12,13] The current state of the art thermoelectric materials are Bi_2Te_3/Sb_2Te_3 superlattices, having $ZT \approx 2.6$ at room temperature.[13] This value is still too low for thermoelectric energy conversion to compete with traditional energy conversion technologies ($ZT > 4$ is required[14]). However, the experimental and theoretical research to date has only considered a limited number of superlattice designs. *It is likely that the thermoelectric performance potential of superlattices has yet to be fully realized.*

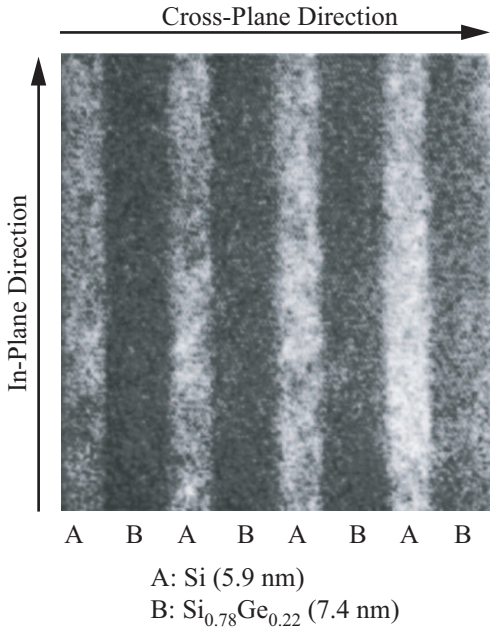

Figure 1: Image of $Si/Si_{0.78}Ge_{0.22}$ superlattice obtained by transmission electron microscopy.[15]

1.2 Literature review

Superlattice thermal conductivity

Superlattices can have high values of the thermoelectric figure-of-merit because of their low cross-plane thermal conductivities, which in some cases, have been observed to be less than the that of an alloy of similar composition.[1–3,5,6,8,16] For some of these cases, the reduction below the alloy thermal conductivity is due to defects and dislocations that result from the strain associated with the lattice mismatch.[17,18] Reductions below the alloy thermal conductivity have also been observed, however, for superlattices without significant defects or dislocations.[1,6,8,18] The effect of the superlattice period length on the experimentally observed thermal conductivity is conflicting. Some studies have found that the thermal conductivity initially decreases with increasing period length until a minimum is reached, beyond which the thermal conductivity increases.[2,3,8] Others have observed the thermal conductivity to increase monotonically with increasing period length.[1,7]

Lattice dynamics calculations,[19–27] and molecular dynamics (MD) simulations[28–34] have been applied to investigate the experimental trends. Traditional lattice dynamics calculations require the assumption of coherent phonon transport. This assumption is only valid when the superlattice period length is not larger than the phonon mean free path. Lattice dynamics calculations performed under this assumption have been used to explain the trend of decreasing thermal conductivity with increasing period length that is sometimes observed for small-period superlattices.[22,24,25,27] This trend is due to the formation of minibands (i.e., frequency gaps) in the phonon dispersion and reductions in the average phonon group velocity as the superlattice period length increases. Most of the traditional lattice dynamics-based approaches make the additional assumption that all phonon modes have the same relaxation time [i.e., the constant relaxation time approximation (CRTA)].[22–27] Broido and Reinecke[21] used an anharmonic lattice dynamics model to obtain the mode-specific relaxation times for Si/Ge superlattices, finding a thermal conductivity trend similar to that obtained under the CRTA. They note, however, that the agreement between the trends is fortuitous and due to a cancelation of errors in the CRTA approach. When the superlattice period length exceeds the phonon mean free path, the phonon transport is incoherent (i.e., phonons scatter at the superlattice interfaces and the phonon properties are distinct within each layer). In this regime, the mechanism of thermal conductivity reduction is phonon scattering at the interfaces. Therefore, the thermal conductivity increases with increasing period length due to decreasing interface density. Simkin and Mahan[19] incorporated the effects of incoherent phonon transport in lattice dynamics calculations by giving the phonons a finite mean free path. This task was accomplished through the addition of an imaginary component to the

wavevector. The resulting model predicted a minimum in the thermal conductivity, corresponding to the period length where phonon transport transitions between the coherent and incoherent regimes. Yang and Chen[20] later expanded this model by adding a second imaginary component to the wavevector to account for diffuse phonon scattering at the interfaces. Qualitative agreement with the experimental trends for GaAs/AlAs superlattices was obtained.

Chen *et al.*[29] applied MD to model Lennard-Jones (LJ) superlattices in order to examine the conditions required to produce a minimum thermal conductivity. It was found that a minimum exists when there is no lattice mismatch, but when the species were given a lattice mismatch of 4%, the thermal conductivity increased monotonically with increasing period length. Daly *et al.*[30] and Imamura *et al.*[31] predicted the effect of interface roughness on the minimum thermal conductivity for model GaAs/AlAs superlattices. Both groups found that the addition of rough interfaces decreased the thermal conductivity and removed the minimum that they observed for superlattices with perfect interfaces. Apart from our recent work,[35] all of the experimental and theoretical effort to date has focused on simple superlattice designs with two layers in the unit cell (e.g., the superlattice shown in Fig. 1).

Thermal boundary resistance

In order to design superlattices with low thermal conductivity, an understanding of the nature of thermal transport across the internal interfaces is required. While experimental methods exist to measure the thermal boundary resistance of isolated interfaces (i.e., where the separation between the interfaces is much greater than the bulk phonon mean free path) where at least one of the species is a metal, there is no method to measure the thermal boundary resistance of semiconductor/semiconductor interfaces.[36,37]

To date, little theoretical work has been performed to predict the thermal boundary resistance for closely-spaced interfaces. For isolated interfaces, the two most common theoretical models for the thermal boundary resistance are the acoustic mismatch and diffuse mismatch models.[38] Both models treat the interface as a two dimensional object and assume that the phonon properties of the bulk materials exists right up to the interface. In the acoustic mismatch model, the mismatch between the interface species is defined by the ratio of the material's acoustic impedances, where the acoustic impedance is defined as the product of the density and sound speed. The phonons are assumed to be continuum elastic waves in the acoustic mismatch model. In the diffuse mismatch model, the degree of mismatch is defined in terms of the bulk phonon density of states. While both models are in reasonable agreement with experiment at temperatures less than $\sim$30 K, they do not predict the

correct magnitude or temperature dependence of the thermal boundary resistance at higher temperatures.[38]

Recent theoretical work has focused on improving the high temperature-accuracy of the acoustic mismatch and diffuse mismatch models by incorporating the effects of exact phonon dispersion,[39] species mixing,[40] and phonon-phonon scattering[41] at the interface. While these models have been shown to be in better agreement with experiment, they typically require fitting parameters and make many of the same assumptions that are required in the original acoustic mismatch and diffuse mismatch models.

Molecular dynamics simulations have also been used to predict thermal transport across isolated interfaces. Stevens *et al.*[42] applied MD (and the direct method) to predict the thermal boundary resistance of isolated interfaces described by the Lennard-Jones potential. It was found that species mixing at the interface decreased the thermal boundary resistance by nearly a factor of two for highly mismatched interfaces. The results also indicated that inelastic phonon scattering is important at high temperature, which may explain the failure of the diffuse mismatch model to predict the correct temperature dependence of the thermal boundary resistance (the diffuse mismatch model assumes elastic scattering events[38]). Molecular dynamics simulations have also been used to model thermal transport across silicon[43] and diamond[44] grain boundaries. Schelling *et al.*[45] applied MD to model the interactions of single phonon wave packets incident on an interface at zero temperature. For long wavelength phonons, the fraction of the incident phonon energy transmitted across the interface was found to be in agreement with the predictions of the acoustic mismatch model. For short wavelength phonons, however, the predictions of the acoustic mismatch model were not in agreement with the simulation results. This discrepancy is due to the invalidity of the continuum elastic waves when the phonon wavelength is on the order of the interatomic distance. In summary, while thermal transport across isolated interfaces has been examined theoretically, the current models are not in agreement with experiment. Furthermore, little effort has been made to examine the effect of closely-spaced interfaces on the thermal boundary resistance.

1.3 Objectives and overview

The objectives of the proposed research are to

- Quantitatively describe thermal transport across isolated and closely-spaced Si/$Si_{1-x}Ge_x$ interfaces,
- Identify metrics for low cross-plane thermal conductivity in superlattices, and
- Design Si/$Si_{1-x}Ge_x$ superlattices for low cross-plane thermal conductivity, desirable in thermoelectric energy conversion.

Silicon- and germanium-based superlattices and interfaces are the focus of this work because (i) $Si_{1-x}Ge_x$ alloys are among the best commercially available thermoelectric materials,[12,13] (ii) the thermal conductivity of Si/Ge superlattices has been observed to be below an alloy of similar composition,[2,5,16] and (iii) suitable interatomic potential functions exist to model silicon and germanium.

Molecular dynamics simulations will be the primary tool used to achieve the research objectives. Details related to the MD simulations and the thermal conductivity and thermal boundary resistance prediction methodologies are presented in Section 2. The prediction methodology is then validated by comparing the MD predicted and experimentally measured thermal conductivities for a variety of silicon and germanium-based samples. This comparison is discussed in Section 3. The proposed research is then discussed in Sections 4 and 5.

In several places in this proposal (e.g., in the comparison between the Green-Kubo and direct thermal conductivity predictions methods, and in motivating the design strategies for reducing the superlattice thermal conductivity), the results of my preliminary study[35] on model Lennard-Jones superlattices are discussed. In this preliminary study, the atomic interactions were described using the Lennard-Jones interatomic potential. The simple form of the this potential allowed for fast simulations, and for the elucidation of phenomena and development of analysis techniques that would not be possible in more complicated systems. The model superlattices were comprised of two species, A and B, that differed only in their mass (i.e., there is no lattice mismatch). Mass ratios, R_m, of two and five were considered, spanning a typical range for superlattices used in application (e.g., the mass ratio between germanium and silicon is 2.6).

2 Molecular dynamics simulations

2.1 Introduction

In an MD simulation, the Newtonian equations of motion are used to predict the time history of the positions and velocities of a set of atoms. Such simulations are an ideal tool for analyzing thermal transport in superlattices and across interfaces because, unlike lattice dynamics-based approaches, no assumptions about the nature of phonon transport (e.g., the CRTA) are required. The only required input is a suitable interatomic potential to determine the total system potential energy, Φ, and net force on each atom (proportional to the spatial derivative of Φ). We use the Stillinger-Weber interatomic potential because it has been used extensively to model thermal transport in bulk and composite materials,[32,45–49] and has been parameterized for both silicon[50] and germanium.[51] In our simulations, the Newtonian equations of motion are integrated using the velocity Verlet algorithm with a time step of 0.55 fs.

2.2 Stillinger-Weber interatomic potential

In the Stillinger-Weber potential, the total system potential energy is the sum of two- and three-body terms, and is given by

$$\Phi = \sum_i \sum_{j>i} v_2(i,j) + \sum_i \sum_j \sum_{k>j} v_3(i,j,k), \tag{1}$$

where v_2 and v_3 are functions of the positions and species of atoms i, j, and k.[50] The first term is a summation over all atom pairs, and the second term is a summation over all triplets with atom i at the vertex. The two-body term is

$$v_2(i,j) = \begin{cases} \epsilon_{ij} A(B y_{ij}^{-p} - y_{ij}^{-q}) \exp[(y_{ij}-c)^{-1}], & \text{if } y_{ij} < c \\ 0 & \text{otherwise,} \end{cases} \tag{2}$$

where A, B, p, and q are constants and c is the nondimensional cutoff radius. The variable y_{ij} is a dimensionless pair separation defined as r_{ij}/σ_{ij}, where $r_{ij} = |\mathbf{r}_i - \mathbf{r}_j|$, and $\mathbf{r}_i$ and $\mathbf{r}_j$ are the positions of atoms i and j. The parameters ϵ_{ij} and σ_{ij} are the energy and length scales for the atomic pair (i,j). The three-body term is

$$v_3(i,j,k) = (\epsilon_{ij}\epsilon_{ik})^{1/2} (\lambda_j \lambda_i^2 \lambda_k)^{1/4} \exp\left[\frac{\gamma}{y_{ij}-c} + \frac{\gamma}{y_{ik}-c}\right] \left(\cos\theta_{jik} + \frac{1}{3}\right)^2, \tag{3}$$

for both $y_{ij} < c$ and $y_{ik} < c$, and zero otherwise. In Eq. (3), θ_{jik} is the angle between atoms i, j, and k with atom i at the vertex, and λ and γ are constants. The energy and length

scales for silicon and germanium were determined by the potential developers by fitting the potential to the crystal cohesive energy and density.[50,51] The constants A, B, p, q, c, λ, and γ were parameterized for silicon by fitting the simulation predictions of the liquid structure (i.e., the radial distribution function) and melting temperature to experimental data while ensuring that the crystal structure with the lowest energy is the diamond lattice.[50] For germanium, the values of A, B, p, q, c, and γ were chosen to be the same as the values for silicon.[51] The value of λ was parameterized by fitting the potential to the zero-temperature elastic constants.[51] We use the mixing rules described by Laradji *et al.* to model the Si-Ge interactions.[52]

2.3 Methods to predict thermal conductivity and thermal boundary resistance

Overview

The Green-Kubo and direct methods are the two most common methods for predicting thermal conductivity using molecular dynamics simulations. While the thermal boundary resistance may also be predicted using a Green-Kubo approach,[53] the direct method is more straight forward for these predictions. In this section, the Green-Kubo method for predicting thermal conductivity and the direct method for predicting thermal conductivity and thermal boundary resistance are discussed. The results of my recent comparison[35] between the Green-Kubo and direct method predictions of the thermal conductivities of model Lennard-Jones superlattices are then presented. To my knowledge, that work represented the first quantitative comparison between the thermal conductivity prediction methods for nanostructures such as superlattices.

Green-Kubo method for predicting thermal conductivity

The Green-Kubo method is an equilibrium molecular dynamics approach that relates the equilibrium fluctuations of the heat current vector, $\mathbf{S}$, to the thermal conductivity, k, via the fluctuation-dissipation theorem. The superlattice thermal conductivity in the l-th direction (either the cross-plane or in-plane direction) is given by[54]

$$k_l = \frac{1}{k_{\mathrm{B}} V T^2} \int_0^\infty \langle S_l(t) S_l(0) \rangle dt, \tag{4}$$

where t is time, V and T are the system volume and temperature, and S_l and $\langle S_l(t) S_l(0) \rangle$ are the l-th components of the heat current vector and the heat current autocorrelation function (HCACF).

There are multiple ways to define the heat current vector.[55–57] The most commonly used definition is

$$\mathbf{S}_1 = \frac{d}{dt}\sum_i \mathbf{r}_i E_i, \tag{5}$$

where E_i is the energy of atom i, and the summation is over all of the atoms in the system. In a solid, where there is no net atomic motion, the heat flux can also be written using the equilibrium positions ($\mathbf{r}_{i,o}$) as

$$\mathbf{S}_2 = \frac{d}{dt}\sum_i \mathbf{r}_{i,o} E_i. \tag{6}$$

The thermal conductivity predictions obtained using both definitions of the heat current vector were compared in my previous work.[35] While both definitions result in the same prediction for the thermal conductivity, the $\mathbf{S_2}$ definition was found to be preferable for solid-phase simulations. This definition is preferred because strong oscillations that are present in the HCACF when using the $\mathbf{S_1}$ definition are avoided. These oscillations were found to complicate the specification of the thermal conductivity in simulations of several different material systems.[33,35,58,59] An additional benefit is that the heat current vector is less computationally expensive with the $\mathbf{S_2}$ definition than the $\mathbf{S_1}$ definition [although not immediately obvious from Eqs. (5) and (6), the $\mathbf{S_1}$ definition requires the calculation of the potential energy of each atom while the $\mathbf{S_2}$ definition does not[35]]. All of the Green-Kubo results presented here were obtained using the $\mathbf{S_2}$ definition of the heat current vector.

Two challenges are encountered when applying the Green-Kubo method to predict the thermal conductivity. The first challenge is properly addressing the effect of the finite simulation cell-size on the predicted thermal conductivity. The thermal conductivity may depend on the size of the simulation cell if there are not enough phonon modes to accurately reproduce the phonon scattering in the associated bulk material. This size dependence is removed by increasing the simulation cell-size until the thermal conductivity reaches a size-independent value.

The second challenge is accurately specifying the converged value of the HCACF integral, which is proportional to the thermal conductivity through Eq. (4). The HCACF and its integral are shown in Fig. 2 for a model $R_m = 2$, 5×5 Lennard-Jones superlattice as an example. Note that specific superlattices are referred to in the format $a \times b$, where a and b are the number of monolayers of the first and second materials. Due to noise in the HCACF that may still exist at long correlation times (even after averaging the results of multiple simulations), it can be difficult to specify the region where the HCACF integral has converged. For the structure shown in Fig. 2, the in-plane and cross-plane thermal conductivities are specified by averaging the HCACF integrals between correlation times of

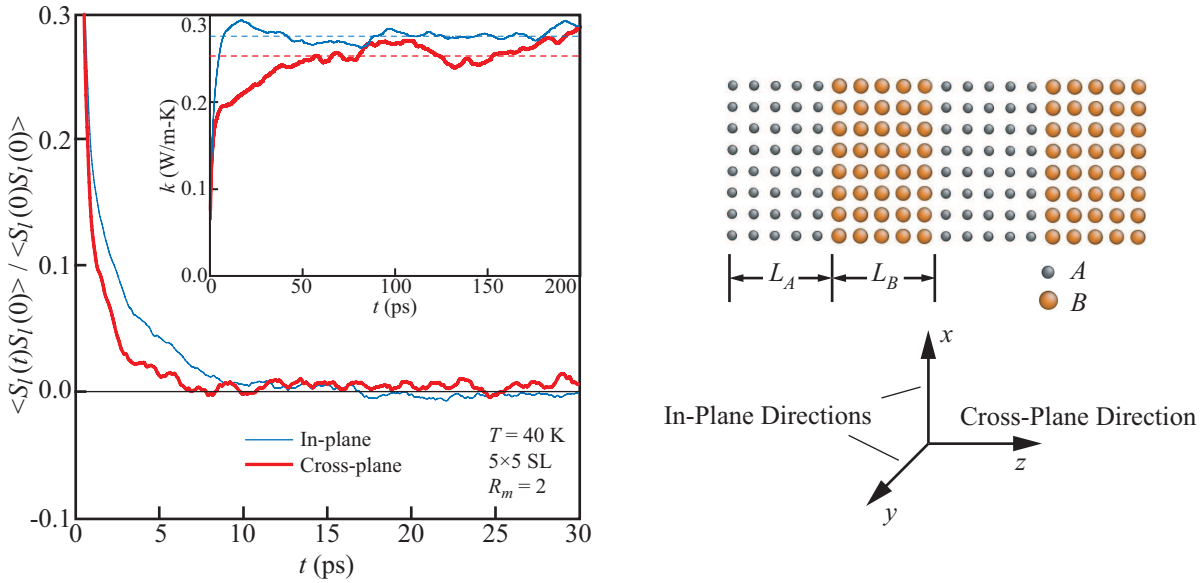

Figure 2: In-plane and cross-plane HCACFs for a model $R_m = 2$, 5×5 Lennard-Jones superlattice (shown on right). The HCACFs have been normalized by their initial values. The integrals of the HCACFs (the thermal conductivity) and their converged values (dashed lines) are shown in the figure inset.

$\sim$50 ps to $\sim$200 ps.

Direct methods for predicting thermal conductivity and thermal boundary resistance

The direct method is a nonequilibrium, steady-state approach for predicting thermal conductivity or thermal boundary resistance.[47,55] A schematic of the direct method simulation cell is shown in Fig. 3. The system consists of a sample bordered by hot and cold reservoirs and fixed boundaries in the z-direction. The fixed boundary regions each contain four layers of fixed atoms in order to prevent the sublimation of the reservoir atoms. Periodic boundary conditions are imposed in the x- and y-directions.

In the direct method, a known heat flux, q, is applied across the sample, causing a temperature profile to develop. The heat flux is generated by adding a constant amount of kinetic energy to the hot reservoir and removing the same amount of kinetic energy from the cold reservoir at every time step using the method described by Ikeshoji and Hafskjold.[60] Example temperature profiles are shown for samples of bulk germanium and an isolated Si/Ge interface in Figs. 3(b) and 3(c). For predictions of the thermal conductivity, the temperature gradient within the sample region is specified and the thermal conductivity is

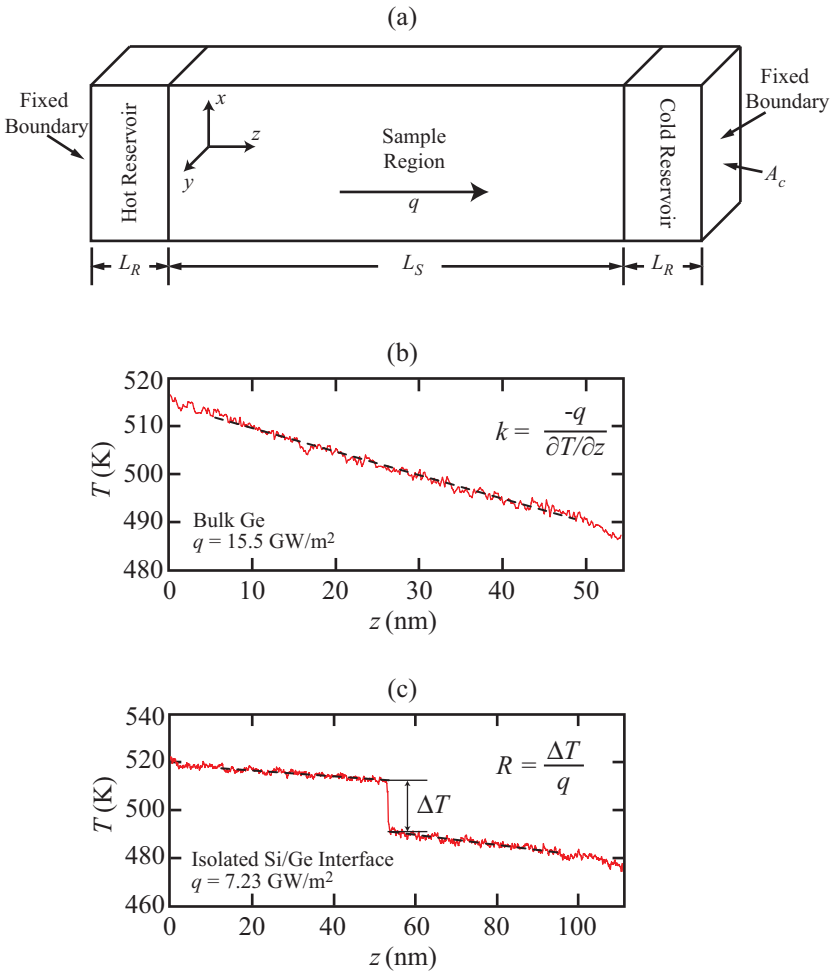

Figure 3: (a) Schematic of the simulation cell used in the direct method. Example temperature profiles for (b) bulk germanium, and (c) an isolated Si/Ge interface.

determined using the Fourier law,

$$k = \frac{-q}{\partial T/\partial z}. \tag{7}$$

For predictions of the thermal boundary resistance, the temperature drop at the interface is specified and the thermal boundary resistance is determined by

$$R = \frac{\Delta T}{q}. \tag{8}$$

As with the Green-Kubo method, a challenge associated with the direct method is obtaining thermal conductivity predictions that are independent of the simulation cell-size. The size of the simulation cell may influence the thermal conductivity when it is not significantly greater than the bulk phonon mean free path. For example, when the sample length, L_S, is on the order of the bulk phonon mean free path, the amount of phonon scattering

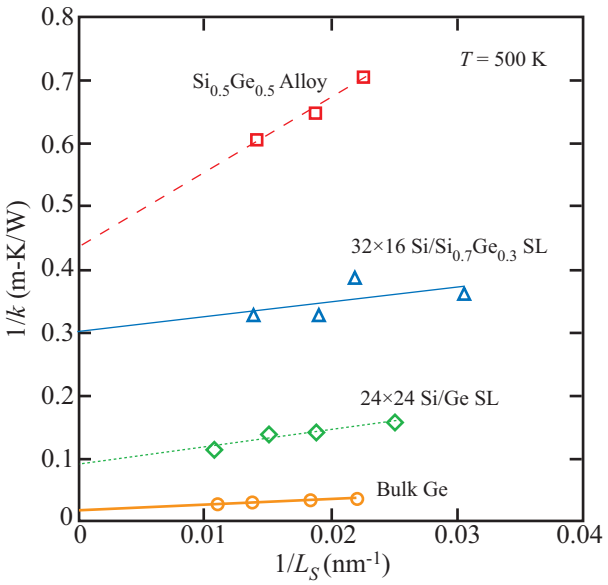

Figure 4: Inverse of the predicted thermal conductivity versus the inverse of the total sample length. Finite-size effects are removed by extrapolating to an infinite system size ($1/L_S \rightarrow 0$).

at the boundaries between the reservoirs and the sample is comparable to that occurring within the sample itself. Furthermore, phonons can potentially travel from the hot reservoir to the cold reservoir without scattering (i.e., ballistic transport). Both of these effects lead to phonon dynamics not representative of the bulk sample and a dependence between the thermal conductivity and the sample length.

For the predictions of the thermal conductivity, we apply the extrapolation procedure described by Schelling *et al.*[47] This procedure is based on the prediction (obtained from Matthiessen's rule and the kinetic theory expression for thermal conductivity) that the inverse of the thermal conductivity decreases linearly with the inverse of the sample length. Therefore, the thermal conductivity corresponding to a sample of infinite length can be determined by extrapolating to the $1/L_S \rightarrow 0$ limit. This extrapolation procedure is illustrated in Fig. 4 for bulk germanium, the $Si_{0.5}Ge_{0.5}$ alloy, and the 24×24 Si/Ge and 32×16 $Si/Si_{0.7}Ge_{0.3}$ superlattices. In all cases, the trend of $1/k$ versus $1/L_S$ is linear, verifying the use of the extrapolation procedure to remove the finite sample size effect. For the predictions of the thermal boundary resistance, the finite sample length-effect is removed by increasing the sample length until size-independent predictions are obtained. We find that the thermal boundary resistance of the $Si/Si_{1-x}Ge_x$ interfaces is not dependent on the sample length when the sample length is greater than or equal to 800 monolayers (∼110 nm).

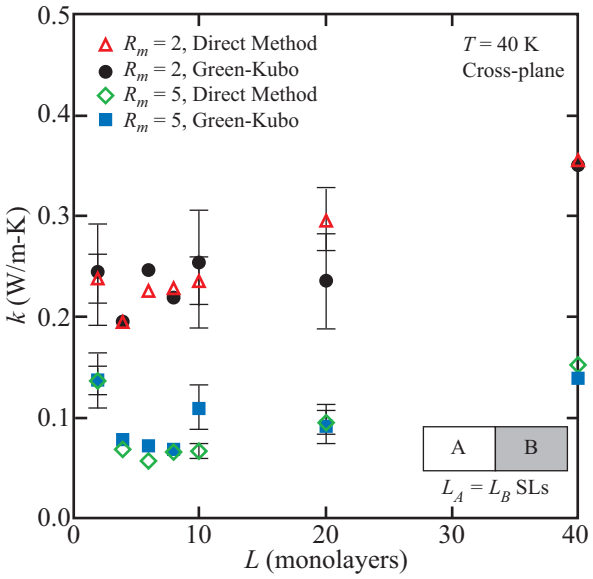

Figure 5: Comparison between the cross-plane thermal conductivity predictions obtained by the Green-Kubo and direct methods for $R_m = 2$ and $R_m = 5$, $L_A = L_B$ Lennard-Jones superlattices. The cross-plane thermal conductivity is plotted as a function of total period length ($L = L_A + L_B$). Error bars have been included for a selection of the results.

Quantitative comparison between the Green-Kubo and direct method predictions of the thermal conductivity

Despite the substantial differences in theory and implementation between the Green-Kubo and direct methods, little work has been conducted to quantitatively compare the thermal conductivity predictions obtained by both methods. One exception is the work of Schelling *et al.*[47] In that work, the thermal conductivity of crystalline silicon at a temperature of 1000 K was predicted using both methods and found to agree to within the measurement uncertainties. Until my recent work on model Lennard-Jones superlattices,[35] however, no such quantitative comparison had been made for nanostructured materials. In this section, the results of that comparison are discussed.

The thermal conductivity prediction methods were compared by predicting the cross-plane thermal conductivity of model Lennard-Jones superlattices with two layers of equal thickness in the unit cell. These results are shown in Fig. 5. Error bars corresponding to the measurement uncertainties (estimated to be $\pm 10\%$ for the direct method and $\pm 20\%$ for the Green-Kubo method) are provided for several points. For all but one point ($R_m = 5$, 5×5), the two sets of predictions are in agreement and neither method consistently underpredicts or overpredicts the other. We conclude, therefore, that either the Green-Kubo method or direct method can be used to predict the superlattice cross-plane thermal conductivity. We

note that the comparison between the thermal conductivity prediction methods was only made for the cross-plane direction because it is difficult to predict the in-plane thermal conductivity using the direct method. This difficulty is due to the very large simulation cell cross-sectional area [A_c, see Fig. 3(a)] that is required to remove the finite cell size-effect on the in-plane thermal conductivity.

Even though the Green-Kubo method has several advantages over the direct method (e.g., it predicts both the in-plane and cross-plane thermal conductivities from one simulation), we prefer to use the direct method for the thermal conductivity predictions. This choice is primarily based on the larger prediction uncertainty associated with the Green-Kubo method than the direct method. All data reported in the remainder of this proposal correspond to predictions obtained using the direct method.

3 Validation of the thermal conductivity prediction methodology

3.1 Samples

In order to ensure that the MD-predicted thermal conductivity trends will be observable in experiment, thermal conductivity predictions were made using the direct method for a series of samples for which experimental data is available.[61] Thermal conductivity predictions were made for bulk Si, bulk Ge, $Si_{1-x}Ge_x$ alloys, and two types of $Si/Si_{1-x}Ge_x$ superlattices. In all of the samples, the atoms are initially located on diamond lattice sites, and the mass of each atom is randomly assigned according to the natural isotope abundance for each species.[62] The two types of superlattice studied are (i) $Si/Si_{0.7}Ge_{0.3}$ superlattices with the Si layer being twice as thick as the alloy layer, and (ii) Si/Ge superlattices with equal Si and Ge layer thicknesses. The 32×16 $Si/Si_{0.7}Ge_{0.3}$ and 24×24 Si/Ge superlattices are shown in Fig. 6. The period length is provided for both superlattices. Note that the interfaces between the species are perfect (no species mixing or defects) and are parallel to the (001) crystallographic plane (i.e., the xy-plane, see Fig. 6). Because MD simulations are only strictly valid in the classical limit, the thermal conductivity predictions are made at a temperature of 500 K. Quantum effects are expected to be negligible at this temperature because it is close to or greater than the experimental Debye temperatures of 658 K and 376 K for Si and Ge.[63]

The thermal conductivity predictions are made using relaxed, zero-stress samples. The zero-stress simulation cell dimensions are determined from separate MD simulations run in the NPT (constant mass, pressure, and temperature) ensemble where the stress in each direction is controlled independently. For bulk Si, bulk Ge, and the $Si_{1-x}Ge_x$ alloys, we find that the zero-stress lattice constant, a, is well-approximated (to within 0.03%) by

$$a(x) = 5.441 + 0.227x + 0.002x^2 \ \text{[Å]}. \tag{9}$$

For the $Si/Si_{1-x}Ge_x$ superlattices, the lattice constant that leads to zero-stress in the in-plane directions (the x- and y-directions) lies between the bulk lattice constants for Si and $Si_{1-x}Ge_x$, leading to a positive in-plane strain in Si and a negative in-plane strain in $Si_{1-x}Ge_x$. For example, the zero-stress in-plane lattice constants for the 32×16 $Si/Si_{0.7}Ge_{0.3}$ and 24×24 Si/Ge superlattices are predicted to be 5.464 Å and 5.564 Å while the bulk lattice constants for Si, Ge, and $Si_{0.7}Ge_{0.3}$ are 5.441 Å, 5.670 Å, and 5.509 Å [see Eq. (9)]. The zero-stress cross-plane (the z-direction) lattice constants are also different from the bulk lattice constants due to the in-plane strain. In Fig. 7, the predicted layer separations for one period of the 32×16 $Si/Si_{0.7}Ge_{0.3}$ and 24×24 Si/Ge superlattices are shown. These results are obtained by

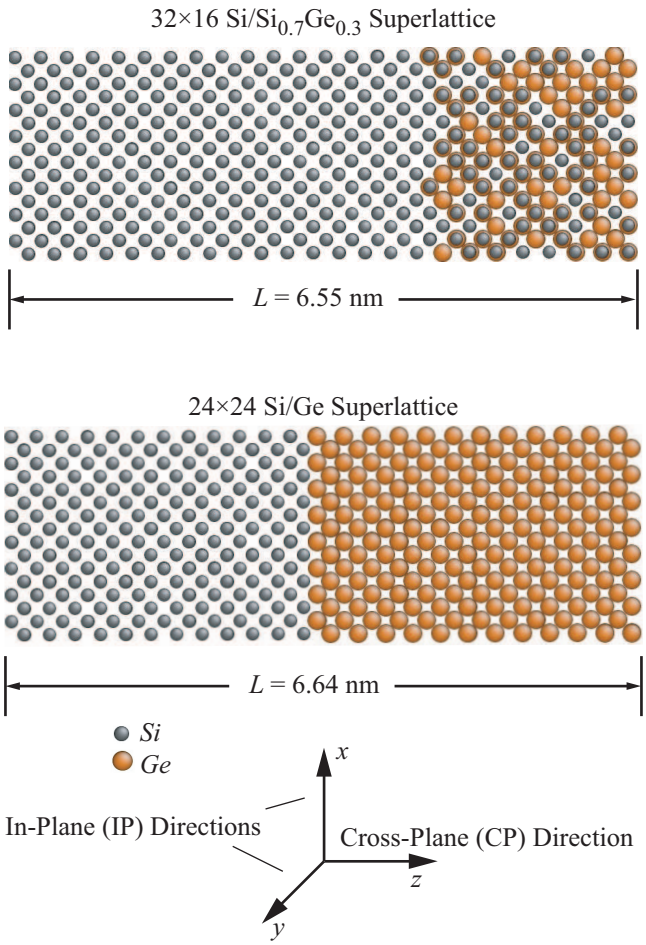

Figure 6: One period of the the 32×16 $Si/Si_{0.7}Ge_{0.3}$ and 24×24 Si/Ge superlattices.

averaging the layer separation data over ten different superlattice periods and 55 ps (1×10^5 time steps). The cross-plane strain is negative in the Si layer and positive in the Ge and $Si_{0.7}Ge_{0.3}$ layers.

The superlattices modeled are symmetrically strained, meaning that the in-plane tensile strain in the Si layer balances the in-plane compressive strain in the $Si_{1-x}Ge_x$ layer. In practice, symmetrically strained superlattices are fabricated by growing (e.g. with molecular beam epitaxy[5,7]) alternating Si and $Si_{1-x}Ge_x$ layers on a substrate that has a lattice constant equal to the average of the bulk Si and $Si_{1-x}Ge_x$ lattice constants. The advantage that symmetrically strained superlattices have over non-symmetrically strained superlattices is that the critical thickness for the formation of misfit dislocations is greater.[64] For example, symmetrically strained Si/Ge superlattices can be grown with layer thicknesses up to ∼5 nm (∼40 atomic layers) while Si/Ge superlattices grown on a Si substrate have a maximum layer thickness of ∼1 nm.[64]

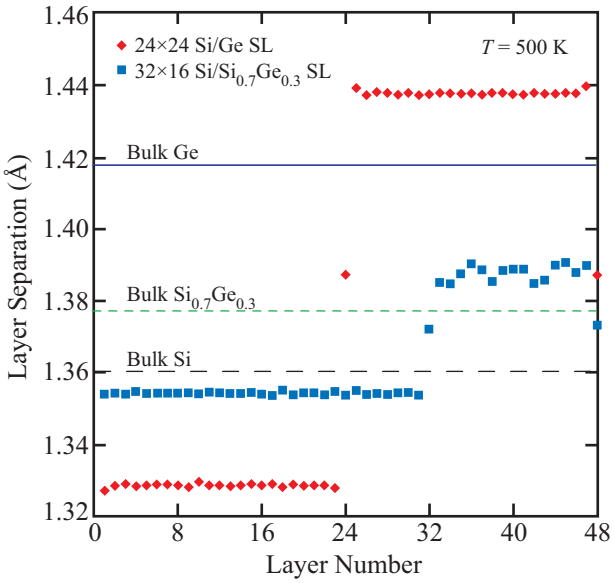

Figure 7: Separation between the atomic layers for one period of the the 32×16 $Si/Si_{0.7}Ge_{0.3}$ and 24×24 Si/Ge superlattices.

3.2 Thermal conductivity predictions and comparison with experiment

Bulk Si, bulk Ge, and $Si_{1-x}Ge_x$ alloy

The thermal conductivity predictions for bulk Si, bulk Ge, and the $Si_{1-x}Ge_x$ alloys at a temperature of 500 K are plotted in Fig. 8 against the atomic fraction of Ge in the unit cell. We predict the thermal conductivities of bulk Si and bulk Ge to be 103±21 W/m-K and 61±12 W/m-K, 35% and 80% greater than the experimental values of 76.2 W/m-K and 33.8 W/m-K.[62] For the $Si_{1-x}Ge_x$ alloys, the thermal conductivity initially decreases with increasing Ge concentration until $x \approx 0.3$, beyond which the thermal conductivity increases with increasing Ge concentration. This trend is in agreement with experimental measurements at a temperature of 300 K.[65] To our knowledge, the thermal conductivity of undoped $Si_{1-x}Ge_x$ alloys at a temperature of 500 K has only been been measured experimentally for $x \approx 0.3$ and $x \approx 0.7$.[66] At these Ge concentrations, the MD-predicted thermal conductivities are 50% and 30% less than the experimental measurements of ∼5-6 W/m-K.[66]

Diffuse and high-scatter limits

The thermal conductivity at the diffuse and high-scatter limits is also provided in Fig. 8. The diffuse limit is an upper bound on the superlattice thermal conductivity. This limit is reached when (i) the phonon scattering is diffuse within the superlattice layers (i.e., the layer

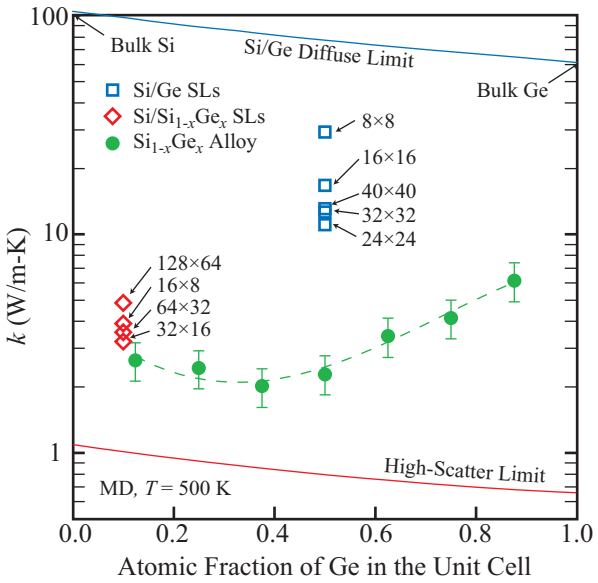

Figure 8: Predicted thermal conductivities for bulk Si, bulk Ge, the $Si_{1-x}Ge_x$ alloys, and the $Si/Si_{0.7}Ge_{0.3}$ and Si/Ge superlattices plotted against the fraction of Ge in the unit cell. A second-order polynomial fit is included through the alloy data to guide the eye. The diffuse and high-scatter limits are provided for comparison.

thicknesses are much greater than the bulk phonon mean free paths), and (ii) the thermal boundary resistance at the superlattice interfaces is negligible compared to the resistance due to conduction within the superlattice layers (also reached in the limit of large layer thicknesses). The cross-plane thermal conductivity for a superlattice with two layers in the unit cell comprised of species A and B at the diffuse limit, $k_{CP,diff}$, is

$$k_{CP,diff} = \frac{t_A + t_B}{t_A k_A^{-1} + t_B k_B^{-1}}, \tag{10}$$

where t_A and t_B are the layer thicknesses, and k_A and k_B are bulk thermal conductivities of species A and B. The diffuse limit shown in Fig. 8 corresponds to that for Si/Ge superlattices.

The high-scatter limit is a lower bound on the thermal conductivity and is based on a model proposed by Cahill *et al.*[67] This limit is reached when all phonons have a mean free path equal to half of their wavelength, corresponding to a material that lacks long range order (e.g., an amorphous phase). Assuming isotropic and linear phonon dispersion, fully excited phonon modes (valid for the classical MD system), and harmonic specific heats, the thermal conductivity at the high-scatter limit, k_{HS}, is

$$k_{HS} = \frac{1}{2}\left(\frac{\pi}{6}\right)^{1/3} k_B n_v^{2/3} \sum_i v_i, \tag{11}$$

where n_v is the atomic number density and v_i is the sound speed (i.e., the phonon group

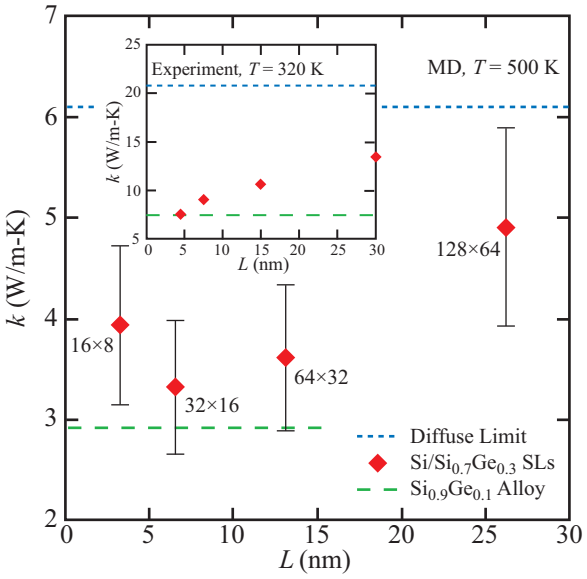

Figure 9: Molecular dynamics-predicted (body) and experimentally measured[7] (inset) thermal conductivities for the $Si/Si_{0.7}Ge_{0.3}$ superlattices. The diffuse limit and the thermal conductivity of an alloy with identical Ge composition are provided for comparison.[7,71]

velocity in the zero-wavevector limit) for polarization i (there are two transverse and one longitudinal polarizations). We estimate v_i for the amorphous phase by scaling the [100] sound speeds for the $Si_{1-x}Ge_x$ alloy by a factor of 0.8 (a typical value for the ratio of the amorphous to crystalline sound speeds for Si and Ge[67,68]). The alloy sound speeds are evaluated using the continuum elastic constants, which we calculate for the Stillinger-Weber potential using the analytical approach described by Cowley.[69] We estimate the elastic constant dependence on the Ge concentration by interpolating between the values for bulk Si and bulk Ge, an approximation that is justified by experimental observations and theoretical predictions.[70] We note that all of the MD-predicted thermal conductivities in Fig. 8 are above the high-scatter limit.

$Si/Si_{0.7}Ge_{0.3}$ superlattices

The cross-plane thermal conductivity predictions for the $Si/Si_{0.7}Ge_{0.3}$ superlattices are plotted against the superlattice period length in Fig. 9. The experimental thermal conductivity measurements obtained by Huxtable *et al.*[7] for $Si/Si_{0.7}Ge_{0.3}$ superlattices at a temperature of 320 K are provided in the inset of Fig. 9 for comparison. Huxtable *et al.* found that the thermal conductivity is nearly independent of temperature between temperatures of 200 K and 320 K. Therefore, we can compare our MD predictions to the experimental results at 320 K by assuming that the thermal conductivity remains temperature-independent up to a

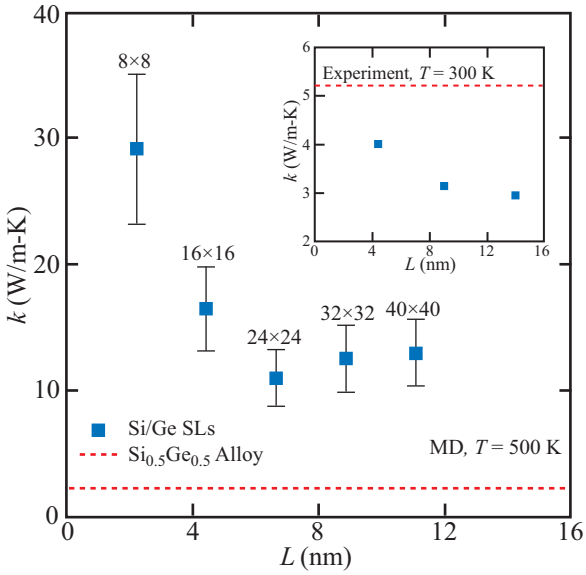

Figure 10: Molecular dynamics-predicted (body) and experimentally measured[5] (inset) thermal conductivity of the Si/Ge superlattices. The diffuse limit and the thermal conductivity of an alloy with identical Ge composition are provided for comparison.[16]

temperature of 500 K.

The predicted thermal conductivities of the $Si/Si_{0.7}Ge_{0.3}$ superlattices are between the diffuse limit and the value for an alloy with the same Ge concentration (i.e., the $Si_{0.9}Ge_{0.1}$ alloy), a finding that is in agreement with the experimental observations. We predict the superlattice thermal conductivity to decrease with decreasing period length until a period length of 6.55 nm (the 32×16 superlattice), beyond which there is a slight increase in the thermal conductivity. Due to the prediction uncertainty, however, we cannot conclude that a minimum exists in the $Si/Si_{0.7}Ge_{0.3}$ superlattice thermal conductivity as a function of period length. We note that thermal conductivity is experimentally observed to decrease monotonically with decreasing period length (see the inset in Fig. 9). This trend is expected when the phonon transport is incoherent across the interfaces due to the increasing interface density (see Section 5.1). For the entire period-length range, the MD predictions are a factor of ~2-3 below the experimental values.

Si/Ge superlattices

The MD predictions for the cross-plane thermal conductivity of the Si/Ge superlattices are shown in Fig. 10 along with the experimental measurements made by Borca-Tasciuc *et al.*[5] The thermal conductivity of alloys with identical Ge concentration are also included for comparison.[16] The MD predictions are made at a temperature of 500 K while the experi-

mental measurements were made at a temperature of 300 K. As with the $Si/Si_{0.7}Ge_{0.3}$ superlattices, we can compare these predictions and measurements due to the weak temperature-dependence of the thermal conductivity observed between temperatures of 200 K and 300 K.[5]

We predict the thermal conductivity of the Si/Ge superlattices to decrease with increasing period length and then to reach a constant value of ∼12 W/m-K for period lengths greater than or equal to 6.64 nm. The trend of decreasing thermal conductivity with increasing period length is also observed in the experimental data of Borca-Tasciuc *et al.* and is indicative of coherent phonon transport (see Section 5.1). The magnitude of the predicted thermal conductivity, however, is a factor of ∼4 greater than the experimental measurements. A major qualitative difference is observed between the MD predictions and experimental measurements as well. We predict the Si/Ge superlattice thermal conductivities to be greater than that of the $Si_{0.5}Ge_{0.5}$ alloy, while experimentally, the opposite trend is observed.

3.3 Summary

The predicted thermal conductivity trends for bulk Si, bulk Ge, the $Si_{1-x}Ge_x$ alloys, and the $Si/Si_{0.7}Ge_{0.3}$ superlattices are in qualitative agreement with the available experimental data. This agreement suggests that the MD predicted thermal conductivity trends will be observable in experiment and that a mapping function (i.e., a correction factor) can be applied to the MD data to improve the prediction accuracy. More experimental data is required to generate such a mapping function. For the Si/Ge superlattices, the predicted period length dependence is in agreement with the experimental observations. There is a major qualitative difference, however, in that the Si/Ge superlattice thermal conductivities are predicted to be greater than an alloy with identical Ge concentration while the opposite trend is observed experimentally. This discrepancy is likely due to the fact that our superlattices have atomically smooth interfaces and are exactly periodic. In realistic samples, there is always some degree of species mixing at the superlattice interfaces. Also, when superlattices are grown experimentally, there may be some deviation in the length of each period. Both of these factors may reduce the ability for phonons to travel coherently through the superlattice and lead to a lower thermal conductivity. We note that the thermal conductivity of the $Si/Si_{0.7}Ge_{0.3}$ superlattices will not be as dependent on the sample quality because the phonon transport is incoherent in these structures. Both effects of species mixing at the Si/Ge interfaces (see Section 4.3 for details on how species mixing will be incorporated into the model) and variations in the period length will be examined in my proposed work.

4 Proposed research: Quantitatively describe thermal transport across $Si/Si_{1-x}Ge_x$ interfaces

4.1 Overview

In order to design superlattices with low thermal conductivity, an understanding of the nature of thermal transport across the interfaces is required. The current models for thermal boundary resistance (e.g., the acoustic mismatch and diffuse mismatch models), however, are not in agreement with experiment at high temperature and require many assumptions about the nature of the phonon scattering (e.g., the diffuse mismatch model assumes bulk material properties and that all phonon scattering is diffuse and elastic[38]). In addition, these models do not properly account for the case of closely-spaced interfaces, where the phonon properties on either side of the interface cannot be assumed to be the same as in the bulk materials. *The objective of this portion of my research is to quantitatively describe the thermal boundary resistance dependence on (i) alloy composition for isolated $Si/Si_{1-x}Ge_x$ interfaces, (ii) distance between closely-spaced Si/Ge interfaces, and (iii) degree of species mixing at the isolated Si/Ge interface.* My preliminary results for the first two items are discussed in Section 4.2. The third item is discussed in Section 4.3 along with additional equilibrium MD simulations that will be used to gain insight into the observed trends.

4.2 Preliminary results

Thermal boundary resistance dependence on alloy composition for the isolated $Si/Si_{1-x}Ge_x$ interface

My preliminary predictions of the thermal boundary resistance of the isolated $Si/Si_{1-x}Ge_x$ interface are shown in Fig. 11 as a function of germanium composition in the alloy layer. The thermal boundary resistance is observed to increase linearly with increasing germanium concentration in the alloy layer until $x \approx 0.8$, beyond which the thermal boundary resistance decreases to the value for the isolated Si/Ge interface. For the isolated Si/Ge interface, the thermal boundary resistance is predicted to be 2.70×10^{-9} m^2-K/W, in good agreement with the value of 2.85×10^{-9} m^2-K/W predicted by Zhao and Freund[46] using a lattice dynamics-based model and the Stillinger-Weber potential. To our knowledge, no predictions of the thermal boundary resistance for $Si/Si_{1-x}Ge_x$ interfaces with $x \neq 1$ have been reported.

The thermal boundary resistance trend is different than that predicted by the acoustic mismatch and diffuse mismatch models, which predict the thermal boundary resistance to increase monotonically with increasing dissimilarity (in terms of acoustic mismatch or

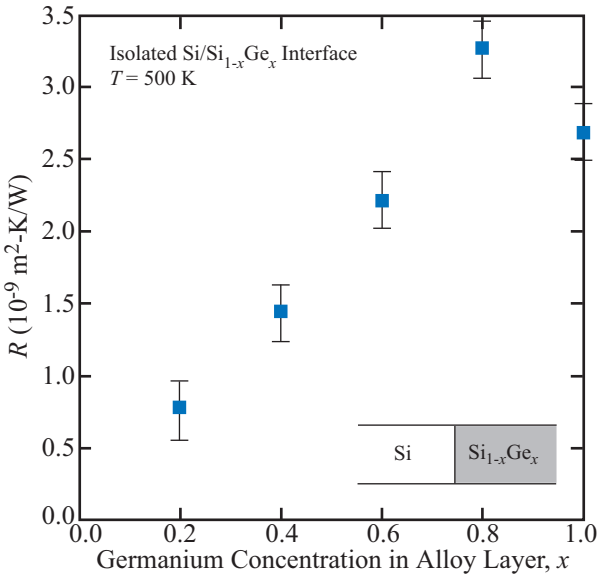

Figure 11: Thermal boundary resistance of an isolated $Si/Si_{1-x}Ge_x$ interface as a function of the atomic fraction of germanium in the alloy layer.

mismatch between the density of states, see Section 1.2) between the interface materials. Equilibrium simulations are discussed in Section 4.3 which will provide insight and a possible explanation for this observed trend. The maximum of the thermal boundary resistance as a function of the alloy composition suggests that there is an optimum alloy composition that can be used to minimize the thermal conductivity of $Si/Si_{1-x}Ge_x$ superlattices (discussed in Section 5). The location of this maximum will be more precisely resolved in my future work by making additional predictions for germanium concentrations between $0.8 < x < 1.0$. In addition, predictions of the thermal boundary resistance will be made for several isolated $Si_{1-y}Ge_y/Si_{1-x}Ge_x$ interfaces. From the results of these simulations, the effect of acoustic mismatch on the thermal boundary resistance will be examined by comparing the thermal boundary resistances of $Si/Si_{1-x}Ge_x$ and $Si_{1-y}Ge_y/Si_{1-x}Ge_x$ interfaces with identical acoustic mismatch.

Thermal boundary resistance dependence on distance between closely-spaced Si/Ge interfaces

In order to examine the effect of distance between closely-spaced Si/Ge interfaces, two types of simulation cells were initially considered. In one case, the simulation cell consists of a germanium layer sandwiched between two large extents of silicon. In the opposite case, a silicon layer is placed between two large extents of germanium. The total thermal resistance, R_{tot}, of these Si/Ge/Si and Ge/Si/Ge structures is plotted in Fig. 12(a) as a function of

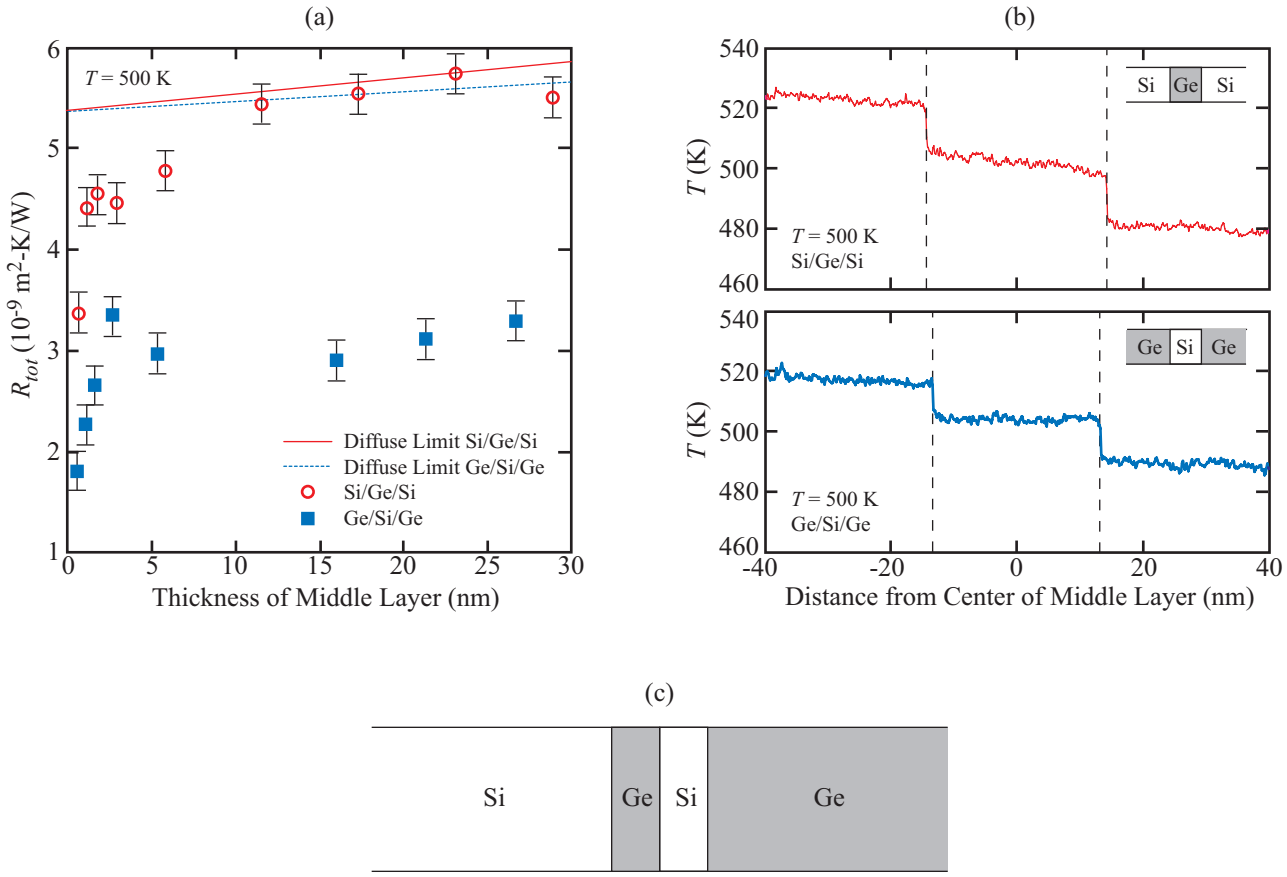

Figure 12: (a) Total thermal resistance (sum of the thermal boundary resistances for the two Si/Ge interfaces and the conduction resistance of the middle layer) of the Si/Ge/Si and Ge/Si/Ge structures as a function of the thickness of the middle layer. (b) Example temperature profiles in the interface region for a Si/Ge/Si (top) and Ge/Si/Ge (bottom) structure. (c) Schematic of a simulation cell containing three closely-spaced interfaces.

the middle layer thickness. The total thermal resistance is the sum of the thermal boundary resistances for both interfaces and the conduction resistance of the middle layer. The diffuse limit (i.e., the total resistance of two isolated Si/Ge interfaces plus the conduction resistance of the middle layer assuming bulk thermal conductivities) is also provided for comparison. For both structures, the total thermal resistance increases with increasing thickness of the middle layer. The thermal resistance of the Ge/Si/Ge structure, however, increases at a slower rate than the Si/Ge/Si structure. This behavior is not yet understood.

Differences between the Si/Ge/Si and Ge/Si/Ge structures are also observed in the temperature profiles. The temperature profiles near the interface region are provided for the Si/Ge/Si and Ge/Si/Ge structures with middle layer thickness of 28.8 nm and 26.6 nm (a thickness of 50 conventional diamond unit cells) in Fig. 12(b). In the Si/Ge/Si structure,

approximately 17% of the total thermal resistance is due to the conduction resistance in the Ge middle layer. In the Ge/Si/Ge structure, the conduction resistance of the Si middle layer is essentially zero, suggesting ballistic phonon transport. The phonon transport is expected to have a ballistic component in these structures because the thickness of the middle layer is smaller than the bulk phonon mean free path (estimated to be ∼50 nm at a temperature of 500 K for both bulk Si and bulk Ge using the kinetic theory expression for thermal conductivity). In order to further explore the effect of interface spacing on the thermal boundary resistance, additional direct method simulations will be run using a simulation cell like that shown schematically in Fig. 12(c). This simulation cell will contain three closely-spaced interfaces. The predicted thermal boundary resistance dependence on interface spacing will be useful in determining if there is an optimum interface spacing to maximize the thermal resistance per unit length and therefore, minimize the superlattice thermal conductivity.

4.3 Proposed work

Thermal boundary resistance dependence on species mixing for the isolated Si/Ge interface

In realistic interfaces, species can diffuse from one side of the interface to the other side, forming a thin alloy region near the interface. The effect of species mixing at the interface on the thermal boundary resistance has previously been predicted for model interface systems.[30,42,72,73] The results, however, are conflicting. Some authors[42,72] have predicted that species mixing decreases the thermal boundary resistance while others[30,73] have predicted the opposite trend. In order to determine the effect of species mixing on thermal transport across the isolated Si/Ge interface, the thermal boundary resistance will be predicted for a series of interfaces with varying thickness of the species mixing region, D. The species profile near the interface will be modeled as

$$x(z) = \frac{1}{2}\left[1 + \tanh\left(\frac{2z}{D}\right)\right], \tag{12}$$

where x is the germanium concentration and z is the distance from the interface. Equation (12) was chosen because it smoothly transitions between the correct asymptotic limits of $x = 0$ (pure silicon) as $z \to -\infty$ and $x = 1$ (pure germanium) as $z \to \infty$ over a distance approximately equal to D. The thermal boundary resistance will be predicted for interface thicknesses of one to ten monolayers, which is on the order of the species mixing region observed in real Si/Ge superlattices.[74]

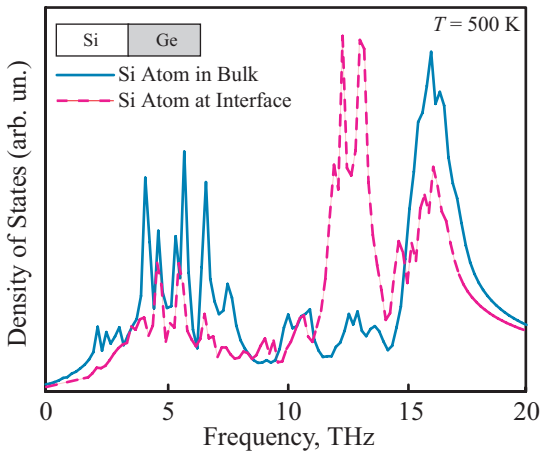

Figure 13: Molecular dynamics-predicted phonon density of states for silicon atoms at the interface and in the bulk region far from the interface.

Identifying the extent of the interface region and determining the role of phonon coherence in thermal transport across interfaces

Equilibrium MD simulations will be used to identify the extent of the interface region and determine the role of phonon coherence in thermal transport across interfaces. From these simulations, important differences in thermal transport behavior between the various types of interfaces considered in my research will be identified. My goal is to use these differences to gain insight to explain the observed thermal boundary resistance trends.

We define the interface extent to be the region surrounding the interface where the phonon density of states is different than that in the bulk regions far from the interface. The phonon density of states will be calculated from the MD simulations by taking the Fourier transform of the velocity autocorrelation function. This calculation can be performed for any atom in the simulation cell, and therefore, the phonon density of states can be determined as a function of distance from the interface. For example, the phonon density of states of a silicon atom located immediately adjacent to the isolated Si/Ge interface is compared to that for a silicon atom in the bulk region far from the interface is shown in Fig. 13. It is clear that the interface strongly modifies the phonon density of states. These calculations will be performed for isolated $Si/Si_{1-x}Ge_x$ interfaces with no interfacial species mixing and isolated Si/Ge interfaces with varying degrees of species mixing. These calculations will also be performed in the center of the middle layer in the Si/Ge/Si and Ge/Si/Ge closely-spaced interface structures.

The role of phonon coherence in thermal transport across interfaces will be explored using equilibrium MD simulations by examining correlations of the planar heat flux. The

planar heat flux can be calculated for any plane in the simulation cell and is defined as the instantaneous flow of heat across that plane. For a system at equilibrium, the planar heat flux fluctuates about zero. My hypothesis is that by taking the cross-correlation of these fluctuations for planes located on either side of the interface, the role of phonon coherence can be examined. I anticipate that interfaces with large values of the thermal boundary resistance will have lower correlation than interfaces with small values of the thermal boundary resistance. I also suspect that the $Si/Si_{1-x}Ge_x$ interfaces with $x < 1$ will have less correlation than the Si/Ge interface due to the lack of well defined phonon modes in the alloy layer (phonons can only exist in an ordered crystal). Therefore, these calculations may lead to an explanation for the observed maximum in the thermal boundary resistance of isolated $Si/Si_{1-x}Ge_x$ interfaces. The correlation between the planar heat flux will also be examined for points on either side of the middle layer in the Si/Ge/Si and Ge/Si/Ge interface structures. From these calculations, the level of phonon coherence across the middle layer can be examined, potentially leading to an explanation for the observed differences between the Si/Ge/Si and Ge/Si/Ge structures.

5 Proposed research: Designing $Si/Si_{1-x}Ge_x$ superlattices for low cross-plane thermal conductivity

5.1 Background

Previous experimental and theoretical studies have demonstrated that superlattices can have very low cross-plane thermal conductivity, a property desirable for thermoelectric energy conversion. To date, only a limited number of superlattice designs have been considered experimentally and theoretically. My hypothesis is that the previously examined superlattices are not the optimal designs to minimize the thermal conductivity. Therefore, the current perspective of the thermoelectric performance of superlattices may be far from optimum. *The objective of this portion of my proposed research is to explore the effect of unit cell design on the thermal transport in superlattices in order to minimize the cross-plane thermal conductivity of $Si/Si_{1-x}Ge_x$ superlattices.* Using a combination of MD simulations, harmonic and anharmonic lattice dynamics calculations, and the Boltzmann transport equation, three strategies will be employed to develop superlattices with low thermal conductivity. These design strategies are discussed in Section 5.2.

5.2 Strategies for reducing the superlattice thermal conductivity

Strategy 1. Optimize the design of superlattices with two layers in the unit cell

The first design strategy is to optimize the design (e.g., alloy composition and layer thicknesses) of superlattices with two layers in the unit cell for superlattices in the incoherent phonon transport regime. In this regime, phonons scatter at the superlattice interfaces. Therefore, the phonon populations are distinct within each layer. The cross-plane thermal conductivity of superlattices with two layers in the unit cell can be predicted in this regime by adding the thermal resistance of the superlattice layers and interfaces in series, i.e.,

$$k_{CP} = \frac{t_A + t_B}{(t_A k_A^{-1} + t_B k_B^{-1}) + 2R_{A|B}}, \tag{13}$$

where $R_{A|B}$ is the thermal resistance of the $A|B$ interface, and t_A, t_B, k_A, and k_B are the thicknesses and thermal conductivities of species A and B. For superlattiecs in the incoherent regime with two layers in the unit cell, Eq. (13) predicts the cross-plane thermal conductivity to decrease with decreasing period length. This trend was observed in my preliminary study of model $R_m = 2$, $L_A = L_B$ Lennard-Jones superlattices for superlattices with period lengths greater than four monolayers (see Fig. 14). These results are presented in Fig. 14.

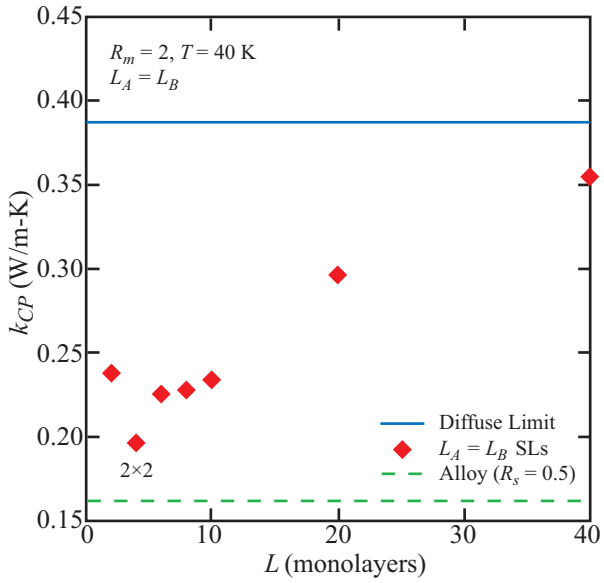

Figure 14: Cross-plane thermal conductivity of the model $L_A = L_B$ Lennard-Jones superlattices plotted as a function of total period length ($L = L_A + L_B$). The thermal conductivity at the diffuse and alloy limits are also provided for comparison.

In this design strategy, I will use the predictions of the thermal boundary resistance (proposed in Section 4.2) and thermal conductivity (described in Section 3.2) to select the superlattice species and layer thicknesses that minimize the cross-plane thermal conductivity given by Eq. (13). As presented in Figs. 8 and 11, the thermal conductivity of $Si_{1-x}Ge_x$ and the thermal boundary resistance of the isolated $Si/Si_{1-x}Ge_x$ interface are functions of the germanium concentration. The thermal boundary resistance is also a function of the layer spacing [see Fig. 12(a)]. There is also a constraint on the layer thickness because the phonon transport will eventually transition from incoherent to coherent when the phonon mean free path exceeds the superlattice period length (this regime is the focus of Strategy 2). The thermal conductivity of the optimized superlattices will then be predicted using MD simulations to examine the validity of the incoherent assumption and Eq. (13).

Strategy 2. Reduce the phonon group velocities and relaxation times using complex layering configurations

The second design strategy is to use complex layering configurations (i.e., unit cells containing more than two layers) to optimize the phonon dispersion and scattering properties in the regime where phonon transport is coherent. The phonon transport is coherent when the bulk phonon mean free path is greater than the superlattice period length. In this regime, the phonon scattering is diffusive (i.e., phonons scatter with other phonons), and the thermal

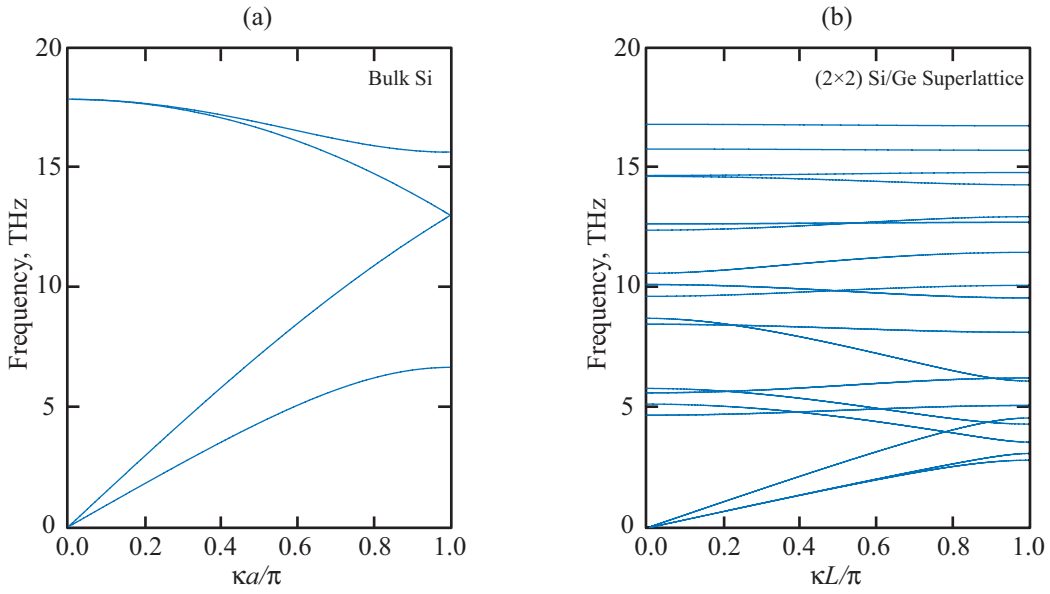

Figure 15: Phonon dispersion curves in the [001] direction (see Fig. 6 for the definition of the coordinate system) for (a) bulk Si and (b) a 2×2 Si/Ge superlattice calculated from harmonic lattice dynamics.

conductivity can be written as

$$k_{CP} = \sum_i c_{v,i} v_{CP,i}^2 \tau_i, \tag{14}$$

where $c_{v,i}$, $v_{CP,i}$, and τ_i are the specific heat, group velocity in the cross-plane direction, and relaxation time for phonon mode i, and the summation is over all available phonon modes. In the classical limit (realized at all temperatures in MD simulations and above the Debye temperature in experiment), every phonon mode is fully excited and the $c_{v,i}$ can be assumed to be phonon mode-independent. Therefore, the thermal conductivity can be reduced by finding superlattice designs that have low phonon group velocities and relaxation times. For superlattices in the coherent regime with two layers in the unit cell, the average phonon group velocity in the cross-plane direction has been predicted to increase with decreasing period length,[21,22,24,25,27] leading to a thermal conductivity that increases with decreasing period length. This trend was observed for the model Lennard-Jones superlattices for period lengths less than or equal to four monolayers [see Fig. 14].

A three step process will be used to quickly search the superlattice unit cell design space for structures that have low phonon group velocities and relaxation times. The search will be limited to Si/Ge superlattices with period lengths less than 5 nm because the phonon transport is believed to be coherent within these structures (see Fig. 10). The first step will be to use lattice dynamics calculations under the harmonic approximation to identify

superlattices with complex layering configurations that have low phonon group velocities. In the harmonic approximation, a Taylor series expansion of the system potential energy about its minimum value is truncated after the second-order term.[33,75] This approach leads to harmonic equations of motion that can be solved numerically (by generating and diagonalizing the dynamical matrix) with calculations taking on the order of seconds. The primary drawback of this approximation, however, is that no information about the phonon scattering (e.g., the phonon relaxation times) can be obtained because the phonon modes are decoupled. In this step, the superlattice designs will be generated using genetic algorithms developed by our collaborator,[33,35] Professor Mahmoud Hussein at the University of Colorado at Boulder. Professor Hussein has previously shown that genetic algorithms can be used to optimize the dispersion properties in phononic crystals.[76] We believe that these algorithms will allow us to efficiently search the supperlattice unit cell design space.

The second step will be to use anharmonic lattice dynamics calculations to predict the phonon relaxation times and the thermal conductivity for the structures already determined to have low phonon group velocities. Anharmonic lattice dynamics calculations introduce the third- and fourth-order terms in the Taylor series expansion of the system potential energy as a perturbation to the harmonic solution.[77] These calculations will require several hours of computation time. If the predicted thermal conductivity is low (compared to other structures encountered in the search of the design space), the superlattice design will be added to a list of structures that will be further explored in step three. We note that one advantage of using anharmonic lattice dynamics for the thermal conductivity prediction is that the contribution of each phonon mode to the total thermal conductivity can be quantified.[77] This quantification will be valuable in assessing the validity of the widely invoked assumption that the acoustic phonons dominate thermal energy transport.[12,78–80]

In the third step, the thermal conductivities of the superlattices predicted by anharmonic lattice dynamics to have low thermal conductivity will also be predicted using MD simulations. Molecular dynamics simulations will only be used in this final step of the design strategy because they are far more computationally expensive than the lattice dynamics approaches, taking on the order of one thousand processor hours to make one prediction. This step is necessary, however, to check the initial assumption of coherent phonon transport, which will be validated if the anharmonic lattice dynamics calculation- and MD-predicted thermal conductivities are in agreement. We have previously demonstrated that these thermal conductivity prediction methods are in agreement to within the prediction uncertainty for the monatomic Lennard-Jones crystal.[77]

The computer codes required to make the harmonic and anharmonic lattice dynamics calculations proposed in this design strategy are available within my research group. I have

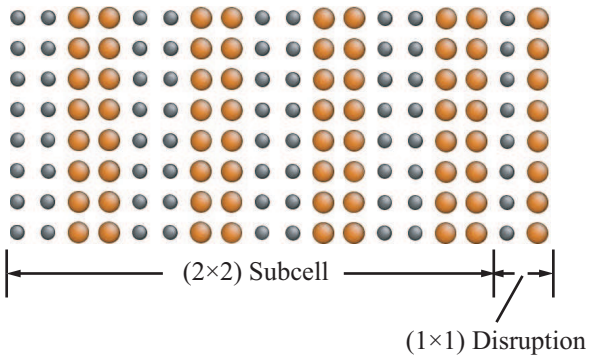

Figure 16: Schematic of the $(2 \times 2)_4(1 \times 1)$ superlattice unit cell that was found in the preliminary Lennard-Jones study to be effective in reducing the thermal conductivity below the minimum observed for the $L_A = L_B$ superlattices (see Fig. 14).[35]

developed a harmonic lattice dynamics computer code and have experience in making the calculations and interpreting the results for a variety of solids described by the Lennard-Jones and Stillinger-Weber potentials.[33,35] The phonon dispersion curves in the [001] direction [see coordinate system definition in Fig. (6)] for bulk silicon and a 2×2 Si/Ge superlattice are shown in Fig. 15 as an example of the types of properties that can be obtained from my code. Note that the superlattice dispersion curves are flatter than the those for bulk silicon, indicating reduced phonon group velocities (the phonon group velocity is equal to the derivative of the phonon angular frequency with respect to the phonon wavevector, κ). For the anharmonic lattice dynamics calculations, I will work in collaboration with Joe Turney, a graduate student in my research group, who has developed a suitable code as part of his Ph.D. work.

Strategy 3. Disrupt the coherent phonon transport in small period superlattices with two layers in the unit cell

The transition between the incoherent and coherent phonon transport regimes produces a minimum in the cross-plane thermal conductivity as a function of period length for superlattices with two layers in the unit cell.[2,3,8,19,29,30,35] For the model $R_m = 2$, $L_A = L_B$ Lennard-Jones superlattices, the minimum was observed for the 2×2 structure (see Fig. 14). The third design strategy consists of adding disruptions to the unit cell of superlattices in which the phonon transport is coherent.

This design strategy was developed during my preliminary work on model Lennard-Jones superlattices.[35] The unit cell of the $(2 \times 2)_4 \times (1 \times 1)$ Lennard-Jones superlattice is shown in Fig. 16 as an example. The thermal conductivity of this disrupted superlattice was predicted to be 0.163 W/m-K, a value that is in the vicinity of the alloy limit (0.162 W/m-K) and

$\sim$20% less than that of the minimum observed for the $L_A = L_B$ superlattices (the 2×2 superlattice, see Fig. 14). The reduced thermal conductivity observed for this structure is attributed to reductions in both the phonon group velocities and the phonon mean free paths in the regime where the phonon transport has both coherent and incoherent qualities. Because the phonon transport is coherent in the 2×2 superlattice, the phonon group velocity is reduced compared to that of the bulk materials.[21,22,24,25,27] The thermal conductivity is then further reduced by adding disruptions to these structures. These disruptions decrease the phonon mean free path below the value that would exist for the normal 2×2 superlattice while maintaining the low group velocity associated with this structure.

In extending this concept of a disrupted superlattice unit cell to the design of $Si/Si_{1-x}Ge_x$ superlattices, MD simulations will be the primary prediction tool because they naturally incorporate the combined effects of incoherent and coherent phonon transport. The procedure will begin by selecting a Si/Ge superlattice with two layers in the unit cell that is in the coherent transport regime. My preliminary calculations (presented in Section 3) and experimental data suggests an appropriate choice is a 16×16 Si/Ge superlattice. I will examine the effects of the spacing between the disruptions and the design of the disruptions on the thermal conductivity. My hypothesis is that in order to have a low thermal conductivity with the disrupted unit cell design, the disruption spacing should be large enough to contain several 16×16 subcells in order to recover the low phonon group velocities associated with the 16×16 superlattice. In addition, the disruption spacing should be on the order of but not less than the phonon mean free path in order to maximize the effect of phonon scattering at the disruptions.

6 Outcomes and schedule

The outcomes of this proposed research will be:

- A prediction of the thermal boundary resistance dependence on (i) alloy composition for isolated Si/$Si_{1-x}Ge_x$ interfaces, (ii) distance between closely-spaced Si/Ge interfaces, and (iii) degree of species mixing at the isolated Si/Ge interface. These are all properties that are not accessible in experiment.
- A description of how the interface extent and coherence of the planar heat flux are influenced by species mixing and alloy composition of the isolated Si/$Si_{1-x}Ge_x$ interface.
- An assessment of the widely invoked assumption in current thermal conductivity models that the acoustic phonons dominate the thermal energy transport.
- A quantification of how species mixing at the superlattice interfaces and deviations in the period length affects phonon coherence and the thermal conductivity of Si/Ge superlattices.
- An understanding of the metrics required to design superlattices for low cross-plane thermal conductivity.
- A list of Si/$Si_{1-x}Ge_x$ superlattice designs predicted to have low cross-plane thermal conductivity that can be fabricated and experimentally characterized.

The schedule for my proposed research is provided in Fig. 17.

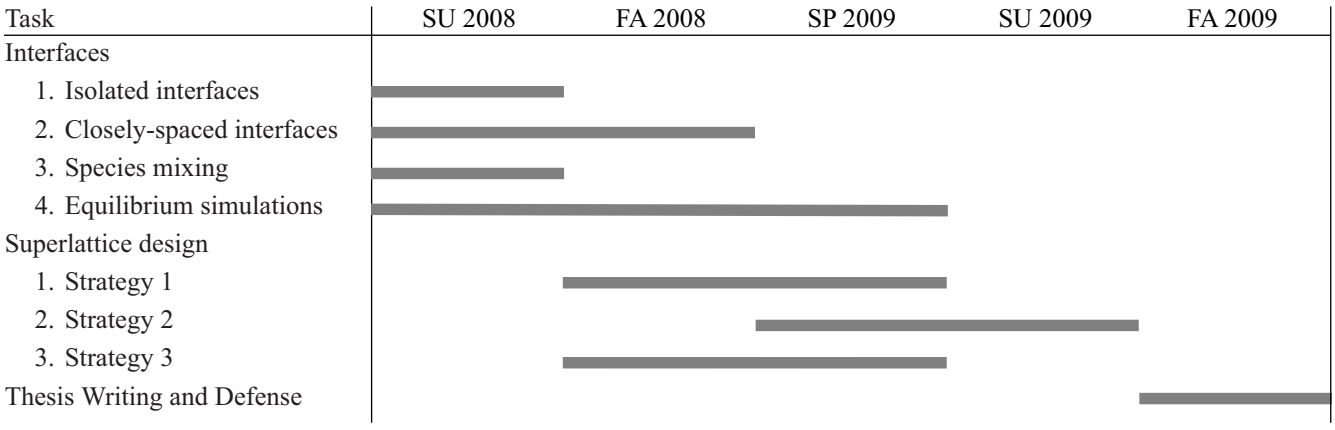

Figure 17: Research timeline.

7 Biographical Sketch

Eric Landry was born and raised in Meriden, CT. He obtained his Bachelor's of Science degree in mechanical engineering from the University of Connecticut in Spring 2005. He entered Carnegie Mellon in Fall 2005 and received his Master's of Science degree in Spring 2007.

Awards

National Science Foundation Graduate Research Fellowship, 2006-present
First place UConn mechanical engineering senior design project, 2005
UConn Honor's Program Sophomore Certificate, 2003
Dominion Nuclear Scholarship, 2003-2005
Francis T. Maloney Scholarship, 2001-2005
Connecticut Innovations Scholarship, 2001-2005
University of Connecticut Merit Scholarship, 2001-2005

Peer-reviewed Journal Publications

1. E. S. Landry and A. J. H. McGaughey, "Molecular dynamics prediction of the thermal conductivity of $Si/Si_{1-x}Ge_x$ superlattices," In preparation.

2. J. E. Turney, E. S. Landry, A. J. H. McGaughey, and C. H. Amon, "Thermal conductivity prediction by anharmonic lattice dynamics calculations and comparison to molecular dynamics methods," In preparation.

3. E. S. Landry, M. I. Hussein, and A. J. H. McGaughey, "Complex superlattice unit cell designs for reduced thermal conductivity," To appear in *Physical Review B*.

4. E. S. Landry, S. Mikkilineni, M. Paharia, and A. J. H. McGaughey, "Nanodroplet Evaporation: A Molecular Dynamics Investigation," *Journal of Applied Physics* **102** 124301 (2007). Paper selected to appear in Virtual Journal of Nanoscale Science & Technology, January 7, 2008 issue.

5. A. J. H. McGaughey, M. I. Hussein, E. S. Landry, M. Kaviany, and G. Hulbert, "Phonon band structure and thermal transport correlation in a layered diatomic crystal," *Physical Review B* **74** 104304-1-12 (2006).

6. A. Chaparro, E. Landry, and B. M. Cetegen, "Transfer function characteristics of bluff-body stabilized, conical V-shaped premixed turbulent propane-air flames," *Combustion and Flame* **145** 290-299 (2006).

Conference Presentations

1. E. J. Terrell, E. Landry, A. McGaughey, and C. Fred Higgs III, "Molecular dynamics simulation of nanoindentation," to be presented by E. T. at IJTC2008, Miami, FL, October 2008.

2. E. S. Landry, M. I. Hussein, and A. J. H. McGaughey, "Designing $Si/Si_{1-x}Ge_x$ Superlattices with Tailored Thermal Transport Properties," presented by E. L. at Spring 2008 MRS Meeting, San Francisco, CA, March 2008.

3. E. S. Landry, T. Matsuura, and A. J. H. McGaughey, "Molecular Dynamics Predictions of the Thermal Boundary Resistance of Isolated and Closely-spaced $Si/Si_{1-x}Ge_x$ Interfaces," poster presented by E. L. at Spring 2008 MRS Meeting, San Francisco, CA, March 2008.

4. E. S. Landry, M. I. Hussein, and A. J. H. McGaughey, "Dielectric Nanocomposite Layering Configurations for Thermal Conductivity Reduction," ASME paper MN2008-47052, presented by M. H. at MN 2008, Sharm El Sheikh, Egypt, January 2008.

5. J. A. Thomas, M. Paharia, E. S. Landry, G. Lee, A. J. H. McGaughey, "Atomistic Water Droplet Simulation," presented by J. T. at DFD07 Meeting of the American Physical Society, Salt Lake City, UT, November 2007.

6. E. S. Landry, M. I. Hussein, and A. J. H. McGaughey, "Molecular dynamics prediction of the thermal conductivity of $Si/Si_{1-x}Ge_x$ superlattices," ASME paper IMECE2007-43177, presented by A. M. at IMECE 2007, Seattle, WA, November 2007.

7. E. S. Landry, M. I. Hussein, and A. J. H. McGaughey, "Molecular dynamics prediction of the thermal conductivity of Si/Ge superlattices," ASME paper HT2007-32152, presented by E. L. at HT 2007, Vancouver, BC, Canada, July 2007.

8. S. Mikkilineni, E. S. Landry, and A. J. H. McGaughey, "Subcritical and supercritical nanodroplet evaporation: A molecular dynamics investigation," ASME paper HT2007-32418, presented by E. L. at HT 2007, Vancouver, BC, Canada, July 2007.

9. E. S. Landry, S. Mikkilineni, and A. J. H. McGaughey, "Subcritical and supercritical nanodroplet evaporation: A molecular dynamics investigation," in *Proceedings of the ILASS Americas 20th Annual Conference on Liquid Atomization and Spray Systems*, presented by A. M. in Chicago, IL, May 2007.

10. A. J. H. McGaughey and E. S. Landry, "Exploration of the superlattice thermal conductivity design space," presented as an invited talk by A. M. at Spring 2007 MRS Meeting, San Francisco, CA, April 2007.

11. E. S. Landry and A. J. H. McGaughey, "Exploration of the superlattice thermal conductivity design space," poster presented at the AVS Western Pennsylvania Chapter's Nanoelectronic Devices and Materials Symposium, Pittsburgh, PA, April 2007.

12. E. S. Landry, M. I. Hussein, and A. J. H. McGaughey, "Superlattice analysis for tailored thermal transport characteristics," ASME paper IMECE2006-13673, presented by E. L. at IMECE 2006, Chicago, IL, November 2006.

13. A. Chaparro, E. Landry, and B. M. Cetegen, "Transfer function characteristics of bluff-body stabilized, conical premixed tubulent propane-air flames," in *Proceedings of the Joint Meeting of the U.S. Sections of the Combustion Institute*, presented by E. L., Philadelphia, PA, March 2005.

References

[1] W. S. Capinski, H. J. Maris, T. Ruf, M. Cardona, K. Ploog, and D. S. Katzer, "Thermal-conductivity measurements of GaAs/AlAs superlattices using a picosecond optical pump-and-probe technique." *Phys. Rev. B* **59** (1999) 8105–8113.

[2] S. Chakraborty, C. A. Kleint, A. Heinrich, C. M. Schneider, J. Schumann, M. Falke, and S. Teichert, "Thermal conductivity in strain symmetrized Si/Ge superlattices on Si(111)." *Appl. Phys. Lett.* **83** (2003) 4184–4186.

[3] J. C. Caylor, K. Coonley, J. Stuart, T. Colpitts, and R. Venkatasubramanian, "Enhanced thermoelectric performance in PbTe-based superlattice structures from reduction of lattice thermal conductivity." *Appl. Phys. Lett.* **87** (2005) 023105.

[4] Y. Ezzahri, S. Dilhaire, S. Grauby, J. M. Rampnoux, W. Claeys, Y. Zhang, G. Zeng, and A. Shakouri, "Study of thermomechanical properties of Si/SiGe superlattices using femtosecond transient thermoreflectance technique." *Appl. Phys. Lett.* **87** (2005) 103506.

[5] T. Borca-Tasciuc, W. Liu, J. Liu, T. Zeng, D. W. Song, C. D. Moore, G. Chen, K. L. Wang, M. S. Goorsky, T. Radetic, R. Gronsky, T. Koga, and M. S. Dresselhaus, "Thermal conductivity of symmetrically strained Si/Ge superlattices." *Superlattices Microstruct.* **28** (2000) 199–206.

[6] T. Borca-Tasciuc, D. W. Song, J. R. Meyer, I. Vurgaftman, M. J. Yang, B. Z. Nosho, L. J. Whitman, H. Lee, R. U. Martinelli, G. W. Turner, M. J. Manfra, and G. Chen, "Thermal conductivity of $AlAs_{0.07}Sb_{0.93}$ and $Al_{0.9}Ga_{0.1}As_{0.07}Sb_{0.93}$ alloys and $(AlAs)_1/(AlSb)_{11}$ digital-alloy superlattices." *J. Appl. Phys.* **92** (2002) 4994–4998.

[7] S. T. Huxtable, *Heat Transport in Superlattices and Nanowire Arrays.* Ph.D. Thesis, University of California, Berkeley, Berkeley, CA (2002).

[8] R. Venkatasubramanian, "Lattice thermal conductivity reduction and phonon localization behavior in superlattice structures." *Phys. Rev. B* **61** (2000) 3091–3097.

[9] D. J. Paul, "Si/SiGe heterostructures: from material and physics to devices and circuits." *Semicond. Sci. Technol.* **19** (2004) R75–R108.

[10] N. Pu, "Ultrafast excitation and detection of acoustic phonon modes in superlattices." *Phys. Rev. B* **72** (2005) 115428.

[11] J. M. Slaughter, D. W. Schulze, C. R. Hills, A. Mirone, R. Stalio, R. N. Watts, C. Tarrio, T. B. Lacuatorto, M. Krumrey, P. mueller, and C. M. Falco, "Structure and performacnce of Si/Mo multilayer mirrors for the extreme ultraviolet." *J. Appl. Phys.* **76** (1994) 2144.

[12] G. Chen, M. S. Dresselhaus, G. Dresselhaus, J.-P. Fleurial, and T. Caillat, "Recent developments in thermoelectric materials." *Int. Mater. Rev.* **48** (2003) 45–66.

[13] H. Bottner, G. Chen, and R. Venkatasubramanian, "Aspects of thin-film superlattice thermoelectric materials, devices, and applications." *MRS Bull.* **31** (2006) 211–217.

[14] F. J. DiSalvo, "Thermoelectric cooling and power generation." *Science* **285** (1999) 703–706.

[15] D. B. Aubertine and P. C. McIntyre, "Influence of Ge concentration and compressive biaxial stress on interdiffusion in Si-rich SiGe alloy heterostructures." *J. Appl. Phys.* **97** (2005) 013531.

[16] S. M. Lee, D. G. Cahill, and R. Venkatasubramanian, "Thermal conductivity of Si-Ge superlattices." *Appl. Phys. Lett.* **70** (1997) 2957–2959.

[17] W. Kim, J. Zide, A. Gossard, D. Klenov, S. Stemmer, A. Shakouri, and A. Majumdar, "Thermal conductivity reduction and thermoelectric figure of merit increase by embedding nanoparticles in crystalline seminconductors." *Physical Review Letters* **96** (2006) 045901.

[18] W. Kim, R. Wang, and A. Majumdar, "Nanostructuring expands thermal limits." *Nanotoday* **2** (2007) 40–47.

[19] M. V. Simkin and G. D. Mahan, "Minimum thermal conductivity of superlattices." *Phys. Rev. Lett.* **84** (2000) 927–930.

[20] B. Yang and G. Chen, "Partially coherent phonon heat conduction in superlattices." *Phys. Rev. B* **67** (2003) 195311.

[21] D. A. Broido and T. L. Reinecke, "Lattice thermal conductivity of superlattice structures." *Phys. Rev. B* **70** (2004) 081310.

[22] B. Yang and G. Chen, "Lattice dynamics study of anisotropic heat conduction in superlattices." *Microscale Thermophys. Eng.* **5** (2001) 107.

[23] S. F. Ren, W. Cheng, and G. Chen, "Lattice dynamics investigations of phonon thermal conductivity of Si/Ge superlattices with rough interfaces." *Microelectron. J.* **100** (2006) 103505.

[24] S. Tamura, Y. Tanaka, and H. J. Maris, "Phonon group velocity and thermal conduction in superlattices." *Phys. Rev. B* **60** (1999) 2627–2630.

[25] A. A. Kiselev, K. W. Kim, and M. A. Stroscio, "Thermal conductivity of Si/Ge superlattices: A realistic model with a diatomic unit cell." *Phys. Rev. B* **62** (2000) 6896–6899.

[26] P. Hyldgaard and G. D. Mahan, "Phonon superlattice transport." *Phys. Rev. B* **56** (1997) 10754–10757.

[27] W. E. Bies, R. J. Radtke, and H. Ehrenreich, "Phonon dispersion effects and the thermal conductivity reduction in GaAs/AlAs superlattices." *J. Appl. Phys.* **88** (2000) 1498–1503.

[28] A. R. Abramson, C.-L. Tien, and A. Majumdar, "Interface and strain effects on the thermal conductivity of heterostructures: A molecular dynamics study." *J. Heat Transfer* **124** (2002) 963–970.

[29] Y. Chen, D. Li, J. R. Lukes, Z. Ni, and M. Chen, "Minimum superlattice thermal conductivity from molecular dynamics." *Phys. Rev. B* **72** (2005) 174302.

[30] B. C. Daly, H. J. Maris, K. Imamura, and S. Tamura, "Molecular dynamics calculation of the thermal conductivity of superlattices." *Phys. Rev. B* **66** (2002) 024301.

[31] K. Imamura, Y. Tanaka, N. Nishiguchi, S. Tamura, and H. J. Maris, "Lattice thermal conductivity in superlattices: Molecular dynamics calculations with a heat reservoir method." *Journal of Physics: Condensed Matter* **15** (2003) 8679–8690.

[32] S. Volz, J. B. Saulnier, G. Chen, and P. Beauchamp, "Computation of thermal conductivity of Si/Ge superlattices by molecular dynamics techniques." *Microelectron. J.* **31** (2000) 815–819.

[33] A. J. H. McGaughey, M. I. Hussein, E. S. Landry, M. Kaviany, and G. M. Hulbert, "Phonon band structure and thermal transport correlation in a layered diatomic crystal." *Phys. Rev. B* **74** (2006) 104304.

[34] C. Chiritescu, D. G. Cahill, N. Nguyen, D. Johnson, A. Bodapati, P. Keblinski, and P. Zschack, "Ultralow thermal conductivity in disordered, layered WSe_2 crystals." *Science* **315** (2007) 351–353.

[35] E. S. Landry, M. I. Hussein, and A. J. H. McGaughey, "Complex superlattice unit cell designs for reduced thermal conductivity." *To appear in Phys. Rev. B* .

[36] R. M. Costescu, M. A. Wall, and D. G. Cahill, "Thermal conductance of epitaxial interfaces." *Phys. Rev. B* **67** (2003) 054302.

[37] R. J. Stevens, A. N. Smith, and P. M. Norris, "Measurment of thermal boundary conductance of a series of metal-dielectric interfaces by the transient thermoreflectance technique." *J. Heat Transfer* **127** (2005) 315–322.

[38] E. T. Swartz and R. O. Pohl, "Thermal boundary resistance." *Review of Modern Physics* **61** (1989) 605–668.

[39] P. Reddy, K. Castelino, and A. Majumdar, "Diffuse mismatch model of thermal boundary conductance using exact phonon dispersion." *Appl. Phys. Lett.* **87** (2005) 211908.

[40] T. Beechem, S. Graham, P. Hopkins, and P. Norris, "Role of interface disorder on thermal boundary conductance using a virtual crystal approach." *Appl. Phys. Lett.* **90** (2007) 054104.

[41] R. S. Prasher and P. E. Phelan, "A scattering-mediated acoustic mismatch model for the prediction of thermal boundary resistance." *J. Heat Transfer* **123** (2001) 105–112.

[42] R. J. Stevens, L. V. Zhigilei, and P. M. Norris, "Effects of temperature and disorder on thermal boundary conductance at solid-solid interfaces: Nonequilibrium molecular dynamics simulations." *Int. J. Heat and Mass Transfer* **50** (2007) 3977–3989.

[43] P. K. Schelling, S. R. Phillpot, and P. Keblinski, "Kapitza conductance and phonon scattering at grain boundaries by simulation." *Journal of Applied Physics* **95** (2004) 6082–6091.

[44] M. A. Angadi, T. Watanabe, A. Bodapati, X. Xiao, O. Auciello, J. A. Carlisle, J. A. Eastman, P. Keblinski, P. K. Schelling, and S. R. Phillpot, "Thermal transport and grain boundary conductance in ultrananocrystalline diamond thin films." *J. Appl. Phys.* **99** (2006) 114301.

[45] P. K. Schelling, S. R. Phillpot, and P. Keblinski, "Phonon wave-packet dynamics at semiconductor interfaces by molecular-dynamics simulation." *Appl. Phys. Lett.* **80** (2003) 2484–2486.

[46] H. Zhao and J. B. Freund, "Lattice-dynamical calculation of phonon scattering at ideal Si-Ge interfaces." *J. Appl. Phys.* **97** (2005) 024903.

[47] P. K. Schelling, S. R. Phillpot, and P. Keblinski, "Comparison of atomic-level simulation methods for computing thermal conductivity." *Phys. Rev. B* **65** (2002) 144306.

[48] A. Bodapati, P. K. Schelling, S. R. Phillpot, and P. Keblinski, "Vibrations and thermal transport in nanocrystalline silicon." *Physical Review B* **74** (2006) 245207.

[49] B. Becker, P. K. Schelling, and S. R. Phillpot, "Interfacial phonon scattering in semiconductor nanowires by molecular-dynamics simulation." *Journal of Applied Physics* **99** (2006) 123715.

[50] F. H. Stillinger and T. A. Weber, "Computer simulation of local order in condensed phases of silicon." *Phys. Rev. B* **31** (1985) 5262–5271.

[51] K. Ding and H. C. Andersen, "Molecular-dynamics simulation of amorphous germanium." *Phys. Rev. B* **34** (1986) 6987–6991.

[52] M. Laradji, D. P. Landau, and B. Dunweg, "Structural properties of $Si_{1-x}Ge_x$ alloys: A Monte Carlo simulation with the Stillinger-Weber potential." *Phys. Rev. B* **51** (1995) 4894–4902.

[53] A. J. H. McGaughey and J. Li, "Molecular dynamics prediction of the thermal resistance of solid-solid interfaces in superlattices." In "Proceedings of IMECE 2006," ASME, paper number IMECE2006-13590.

[54] D. A. McQuarrie, *Statistical Mechanics*. University Science Books, Sausalito (2000).

[55] A. J. H. McGaughey and M. Kaviany, "Phonon transport in molecular dynamics simulations: Formulation and thermal conductivity prediction." In G. A. Greene, Y. I. Cho, J. P. Hartnett, and A. Bar-Cohen (eds.), "Advances in Heat Transfer, Volume 39," Elsevier (2006) 169–255.

[56] A. J. C. Ladd, B. Moran, and W. G. Hoover, "Lattice thermal conductivity: A comparison of molecular dynamics and anharmonic lattice dynamics." *Phys. Rev. B* **34** (1986) 5058.

[57] J. Li, *Modeling Microstructural Effects on Deformation Resistance and Thermal Conductivity*. Ph.D. Thesis, Massachusetts Institute of Technology, Cambridge, MA (2000).

[58] J. Che, T. Cagin, W. Deng, and W. A. Goddard III, "Thermal conductivity of diamond and related materials from molecular dynamics simulations." *J. Chem. Phys.* **113** (2000) 6888–6900.

[59] A. J. H. McGaughey and M. Kaviany, "Thermal conductivity decomposition and analysis using molecular dynamics simulations. Part II. Complex silica structures." *Int. J. Heat Mass Transfer* **47** (2004) 1799–1816.

[60] T. Ikeshoji and B. Hafskjold, "Non-equilibrium molecular dynamics calculation of heat conduction in liquid and through liquid-gas interface." *Molecular Physics* **81** (1994) 251–261.

[61] E. S. Landry and A. J. H. McGaughey, "Molecular dynamics prediction of the thermal conductivity of $Si/Si_{1-x}Ge_x$ superlattices." *In preparation* .

[62] D. R. Lide (ed.), *CRC Handbook of Chemistry and Physics, Internet Version 2007, (87th Edition), http://www.hbcpnetbase.com*. Taylor and Francis, Boca Raton, FL (2007).

[63] W. S. Capinski, H. J. Maris, E. Bauser, I. Silier, M. Asen-Palmer, T. Ruf, M. Cardona, and E. Gmelin, "Thermal conductivity of isotopically enriched Si." *Appl. Phys. Lett.* **71** (1997) 2109–2111.

[64] T. P. Pearsall, "Strain symmetrisation for ultrathin sige superlatices." In E. Kasper and K. Lyutovich (eds.), "Properties of Silicon Germanium and SiGe:Carbon," INSPEC, The Institution of Electrical Engineers (2000) 91–93.

[65] P. D. Maycock, "Thermal conductivity of silicon, germanium, III-V compounds, and III-V alloys." *Solid-State Electronics* **10** (1967) 161–168.

[66] B. Abeles, "Lattice thermal conductivity of disordered semiconductor alloys at high temperatures." *Physical Review* **131** (1963) 1906–1911.

[67] D. G. Cahill, S. K. Watson, and R. O. Pohl, "Lower limit to the thermal conductivity of disordered crystals." *Phys. Rev. B* **46** (1992) 6131–6140.

[68] M. G. Holland, "Analysis of lattice thermal conductivity." *Phys. Rev.* **132** (1963) 2461–2471.

[69] E. R. Cowley, "Lattice dynamics of silicon with empirical many-body potentials." *Phys. Rev. Lett.* **23** (1988) 2379–2381.

[70] S. P. Baker and E. Arzt, "Elastic stiffness constants of sige." In E. Kasper and K. Lyutovich (eds.), "Properties of Silicon Germanium and SiGe:Carbon," INSPEC, The Institution of Electrical Engineers (2000) 91–93.

[71] J. P. Dismukes, L. Ekstrom, E. F. Steigmeier, I. Kudman, and D. S. Beers, "Thermal and electrical properties of heavily doped Ge-Si alloys up to 1300 K." *J. Appl. Phys.* **35** (1964) 2899–2907.

[72] D. Kechrakos, "The role of interface disorder in thermal boundary conductivity between two crystals." *J. Phys: Condens. Matter* **3** (1991) 1443–1452.

[73] C. Twu and J. Ho, "Molecular-dynamics study of energy flow and the kapitza conductance across an interface with imperfection formed by two dielectric thin films." *Phys. Rev. B* **67** (2003) 205422.

[74] Y. L. Soo, G. Kioseoglou, S. Huang, S. Kim, Y. H. Kao, Y. H. Peng, and H. H. Cheng, ""Inverted hut" structure of Si-Ge nanocrystals studied by extended x-ray absorption fine structure method." *Appl. Phys. Lett.* **78** (2001) 3684–3686.

[75] M. T. Dove, *Introduction to Lattice Dynamics*. Cambridge University Press, Cambridge (1993).

[76] M. I. Hussein, K. Hamza, G. M. Hulbert, and K. Saitou, "Multi-objective evolutionary optimization of periodic layered materials for desired wave dispersion characteristics." *Structural and Multidisciplinary Optimization* **31** (2006) 60–75.

[77] J. E. Turney, E. S. Landry, A. J. H. McGaughey, and C. H. Amon, "Thermal conductivity prediction by anharmonic lattice dynamics calculations and comparison to molecular dynamics methods." *In preparation* .

[78] G. Chen, "Thermal conductivity and ballistic-phonon transport in the cross-plane direction of superlattices." *Phys. Rev. B* **57** (1998) 14958.

[79] T. Zeng and G. Chen, "Phonon heat conduction in thin films: Impacts of thermal boundary resistance and internal heat generation." *J. Heat Transfer* **123** (2001) 340–347.

[80] E. Ziambaras and P. Hyldgaard, "Phonon Knudsen flow in nanostructured semiconductor systems." *J. Appl. Phys.* **99** (2006) 054303.